A Parametric Moving Target Detector for Distributed MIMO Radar in Non-Homogeneous Environment

Pu Wang, *Member, IEEE*, Hongbin Li, *Senior Member, IEEE*, and Braham Himed, *Fellow, IEEE*

***Abstract*—This paper considers moving target detection (MTD) with distributed multi-input multi-output (MIMO) radars in non-homogeneous environments, where the received disturbance signal (clutter and noise) exhibits non-homogeneity in not only *power* but also *covariance structure* from one transmit-receive (TX–RX) antenna pair to another as well as across different test cells. To address this problem, we introduce a parametric approach by employing a set of distinctive auto-regressive (AR) models, one for each TX–RX pair, to model the non-homogeneous disturbance signals. We develop a parametric generalized likelihood ratio test (PGLRT), referred to as the MIMO-PGLRT detector, for MTD in distributed MIMO radars. The MIMO-PGLRT detector, which consists of local adaptive subspace detection, non-coherent combining using local decision variables, and a global threshold comparison, is shown to asymptotically achieve constant false alarm rate (CFAR). We also investigate the target velocity estimation problem, an integral part of MTD, and develop its maximum likelihood estimator. The Cramér–Rao bound, in both the exact and asymptotic forms, respectively, is examined to shed additional light to the problem. Numerical results are presented to demonstrate the effectiveness of the proposed methods.**

***Index Terms*—Auto-regressive process, distributed multiple-input multiple-output (MIMO) radar, moving target detection, non-homogeneous clutter, velocity estimation.**

I. Introduction

A distributed multi-input multi-output (MIMO) radar employs widely separated antennas within the transmit and, respectively, receive aperture. The transmit antennas probe a radar scene using multiple orthogonal waveforms which are separated at each receive antenna by matched filter processing [1]–[4]. A distributed MIMO radar allows one to exploit the *spatial or geometric diversity* to enhance target detection [3]–[15]. In particular, radar targets often exhibit significant azimuth-selective backscattering with tens of dB of fluctuation in their radar cross section (RCS) [16]. As a result, it would be difficult for a traditional monostatic or bistatic radar to detect such targets, if the sensors are unfavorably located.

Manuscript received April 06, 2012; revised April 06, 2012 and January 12, 2013; accepted January 18, 2013. Date of publication February 05, 2013; date of current version April 09, 2013. The associate editor coordinating the review of this manuscript and approving it for publication was Prof. Pascal Larzabal. The work was supported by a subcontract with Dynetics, Inc., for work supported by the Air Force Research Laboratory (AFRL) under Contract FA8650-08-D-1303.

P. Wang and H. Li are with the Department of Electrical and Computer Engineering, Stevens Institute of Technology, Hoboken, NJ 07030 USA (e-mail: pwang@ieee.org; hli@stevens.edu).

B. Himed is with AFRL/RYMD, Dayton, OH 45433 USA (e-mail: Braham.Himed@wpafb.af.mil).

Color versions of one or more of the figures in this paper are available online at http://ieeexplore.ieee.org.

Digital Object Identifier 10.1109/TSP.2013.2245323

The spatial diversity of distributed MIMO radar was first discussed in [3] for stationary target detection and later extended in [4] for moving target detection (MTD). The focus of [3] was to establish the detection diversity gain, and clutter was ignored. In a latter work [4], [7], the effect of clutter was included for MTD. It was shown that distributed MIMO radar systems can provide significant performance gain over traditional phased array radar systems. However, the clutter was assumed to be spatially *homogeneous*, i.e., the clutter covariance matrix is identical for all transmit-receive (TX-RX) pairs and for all resolution cells. For adaptive detection, it was suggested to estimate the clutter covariance matrix using training data from adjacent resolution cells, provided that the clutter is homogeneous across these cells. Recently, target detection/localization with the distributed MIMO radar under a phase synchronization mismatch and, respectively, with imperfect signal separation was studied in [9], [12]–[14].

Unlike most previous efforts which deal with MTD in a homogeneous environment, we consider here the problem with *non-homogeneous* clutter, which arises from the multi-static transmitter-receiver configuration inherent in distributed MIMO radars. There are two types of non-homogeneity in such systems. First, for the same resolution cell, the clutter observed by different TX-RX antenna pairs may exhibit non-homogeneous covariance structure (speckle) as well as non-homogeneous power level (texture) due to azimuth-selective backscattering of the clutter scatterers. Second, the clutter covariance structure and power level may also vary significantly across resolution cells in a neighborhood, thus compromising the availability of homogeneous training data from adjacent resolution cells. We introduce a parametric auto-regressive (AR) model based approach aimed to address the first type of non-homogeneity. In particular, we employ a set of different AR processes for clutter observed by different TX-RX pairs, and these independent AR processes are capable of modeling variations in both clutter structure and power level across different probing-observing angles in a distributed MIMO radar. Since the AR processes can be efficiently estimated from the test signal itself (details of estimation in Section IV), there is no need to draw training data from adjacent resolution cells, thus circumventing the second type of non-homogeneity.

Our parametric approach is notably different from [15], where a subspace approach was introduced for MTD with distributed MIMO radars in clutter with non-homogeneous power. Specifically, [15] argues that in MIMO systems where the Doppler spectrum of the clutter is band-limited with a relative small bandwidth around the zero frequency, the clutters seen by different TX-RX pairs can be expanded by the

Fourier bases and share a common Fourier subspace. Since the Fourier coefficients are not identical from one TX-RX pair to another, the subspace approach can handle clutter power (texture) variations across the antenna pairs; however, it cannot deal with clutter with non-homogeneous covariance structure (speckle) due to the common subspace imposed to all clutters. In contrast, the current work is to address MTD in clutter with not only non-homogeneous power but also non-homogeneous covariance structure.

Following the proposed modeling approach, we develop a parametric generalized likelihood ratio test, referred to as the MIMO-PGLRT detector, for the MIMO radar MTD problem. Our development is carried out in a two-step approach. First, we assume that the target velocity is known and derive the test statistic of the proposed detector. Then, we examine explicitly the target velocity estimation problem. This approach keeps our discussions clear and organized. The assumption is also justified by the standard practice in radar detection, whereby the uncertainty region of the target velocity or Doppler frequency is divided into small cells and target detection is performed on each cell one by one. Conditioned on a known target velocity, the proposed detector performs local adaptive subspace detection, non-coherent combining using local decision variables, and finally a global threshold comparison. Statistical analysis shows that the MIMO-PGLRT detector is an asymptotically constant false alarm rate (CFAR) detector. For the estimation problem, our main results include the development of the maximum likelihood (ML) velocity estimator and Cramér-Rao bound (CRB) analysis. The CRB is derived in both the exact form and an asymptotic form. The latter sheds additional light to the target velocity estimation problem in distributed MIMO radars. It is also computationally more efficient to compute than the exact CRB.

The rest of the paper is organized as follows. The signal model is introduced in Section II. The MIMO-PGLRT detector is developed in Section III. Target velocity estimation and CRB analysis are given in Section IV. Simulation results are provided in Section V, followed by conclusions in Section VI.

II. Signal Model

Consider a distributed MIMO radar system with M transmit antenna elements and N receive antenna elements. The transmit and receive antennas are assumed to be on stationary platforms. We use the standard assumption for MIMO radars that the M transmit antennas probe a common area of interest using M orthogonal waveforms [3], [4]. Pulsed transmission is employed as in standard Doppler radars [16]. Each transmitter sends a succession of K periodic pulses, i.e., K repetitions of an orthogonal waveform, over a coherent processing interval (CPI). Each receiver employs a bank of M matched filters corresponding to the M orthogonal waveforms. The matched filter output is sampled at the pulse rate via slow-time sampling. Let $\mathbf{x}_{mn} \in \mathbb{C}^{K\times 1}$ denote the vector formed by the $K \times 1$ samples of the matched filter output (within a CPI) at the n-th receiver matched to the m-th transmitter. The problem of interest is to detect if a moving target is present in the cell of interest (test cell) using the observations $\{\mathbf{x}_{mn}\}$.

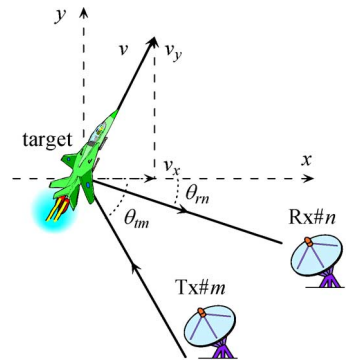

Fig. 1. Transmit-receive (TX-RX) pair geometry.

Specifically, the problem involves the following hypothesis testing [4], [7], [8], [10]:

$$\begin{aligned} H_0: &\quad \mathbf{x}_{mn} = \mathbf{c}_{mn} + \mathbf{w}_{mn}, \\ H_1: &\quad \mathbf{x}_{mn} = \alpha_{mn}\mathbf{s}(f_{mn}) + \mathbf{c}_{mn} + \mathbf{w}_{mn}, \\ &\qquad n = 1,\ldots,N; m = 1,\ldots,M, \end{aligned} \tag{1}$$

where $\mathbf{c}_{mn}$ denotes the clutter, $\mathbf{w}_{mn}$ the noise, $\mathbf{s}(f_{mn})$ the signal vector caused by the target Doppler frequency f_{mn}, and α_{mn} the unknown signal amplitude. Henceforth, we also refer to $\mathbf{s}(f_{mn})$ as the "steering vector" following an analogy from array signal processing.

The unknown Doppler frequency is due to target motion. The moving target has a velocity denoted by its x- and y-component $(v_x, v_y) \triangleq \mathbf{v}$, assuming a 2-dimensional (2-D) motion. This motion is observed as different Doppler frequencies at different TX-RX antenna pairs. Using the geometry depicted in Fig. 1, the normalized Doppler frequency f_{mn} is given by [1], [4], [17]

$$f_{mn} = \frac{T_{\mathrm{PRI}}}{\lambda}\left[v_x(\cos\theta_{tm}+\cos\theta_{rn}) + v_y(\sin\theta_{tm}+\sin\theta_{rn})\right], \tag{2}$$

where λ denotes the wavelength and T_{PRI} the pulse repetition interval (PRI). The signal steering vector, which is formed over the reception of K coherent pulses, is given by

$$\mathbf{s}(f_{mn}) = \left[1 \quad e^{-j2\pi f_{mn}} \quad \cdots \quad e^{-j2\pi f_{mn}(K-1)}\right]^T. \tag{3}$$

The unknown signal amplitude α_{mn} is related to the target radar cross section (RCS). In general, it varies significantly with the aspect angle, due to the azimuth-selective backscattering [3], [4], [16]. As such, in our data model, α_{mn} is assumed to be different for different TX-RX antenna pairs.

The sum $\mathbf{d}_{mn} = \mathbf{c}_{mn} + \mathbf{w}_{mn}$ is referred to as the disturbance signal. The clutter components $\mathbf{c}_{mn}$ contain reflections from stationary (e.g., ground, buildings) and slow moving objects (e.g., grass, forest) within the considered test cell, while the noise components $\mathbf{w}_{mn}$ are receiver thermal noise. We assume $\mathbf{d}_{mn}$ is Gaussian distributed with zero mean and covariance matrix $\mathbf{R}_{d,mn}$, i.e., $\mathbf{d}_{mn} \sim \mathcal{CN}(\mathbf{0}, \mathbf{R}_{d,mn})$, and $\mathbf{R}_{d,mn} = \mathbf{R}_{c,mn} + \mathbf{R}_{w,mn}$, where $\mathbf{R}_{c,mn}$ and $\mathbf{R}_{w,mn}$ denote the covariance matrices of the clutter and noise components, respectively. Due to the non-homogeneity across different TX-RX pairs, we

have $\mathbf{R}_{d,mn} \neq \mathbf{R}_{d,m'n'}$, if $m \neq m'$ and/or $n \neq n'$ [15]. Moreover, for a given TX-RX pair, the disturbances are also non-homogeneous for different resolution cells [15].

To account for the non-homogeneity across TX-RX pairs for one resolution cell, we use a set of AR processes to model the disturbance signal seen by different TX-RX pairs. There is a rich literature of using AR processes to model disturbances in radar and sonar systems [18]–[23]. It has been found from numerous experimentally measured data that AR processes can be used to accurately and efficiently approximate radar disturbances with a model order between 2 and 5 [18], [22]. Modeling of non-stationary X-band sea-clutter using the AR model was considered in [23], which shows that an model order of 3 is enough to capture the relationship between the long-wave evolution and the variation of the speckle spectrum shape parameters, such as texture, Doppler centroid and bandwidth. Herein, we use a set of MN different AR processes to model the disturbances at the MN TX-RX pairs:

$$d_{mn}(k) = -\sum_{p=1}^{P_{mn}} a_{mn}(p) d_{mn}(k-p) + \varepsilon_{mn}(k), \quad k = 1, 2, \cdots, K, \quad (4)$$

where $d_{mn}(k)$ denotes the k-th slow-time sample of the disturbance for the (m,n)-th TX-RX pair, $\varepsilon_{mn}(k) \sim \mathcal{CN}(0, \sigma_{mn}^2)$ the zero-mean driving noise with variance σ_{mn}^2, $a_{mn}(p)$ the p-th AR coefficient, and P_{mn} the AR model order.

III. Parametric GLRT for MIMO-MTD

In this section, we first assume that the target velocity $\mathbf{v}$ is known. It is standard in radar signal detection to divide the uncertainty region of the target velocity or Doppler frequency into small cells and each is tested for the presence of target [16]. Therefore, we will drop the dependence of $\mathbf{s}$ on $\mathbf{v}$ herein. We also briefly discuss the issue of unknown $\mathbf{v}$ in detection, but the estimation of $\mathbf{v}$ is fully addressed in Section IV.

The MIMO-PGLRT detector is developed based upon the GLRT principle, which requires the maximum likelihood estimates (MLEs) of the unknown parameters including the target amplitudes α_{mn}, the driving noise variances σ_{mn}^2, and the AR coefficients $\mathbf{a}_{mn} = [a_{mn}(1), \cdots, a_{mn}(P_{mn})]^T$ under both hypotheses. Due to statistical independence across multiple TX-RX pairs, the MIMO-PGLRT detector takes the form of

$$T_{\text{MIMO-PGLR}} = \frac{\prod_{m,n} \max_{\alpha_{mn}, \mathbf{a}_{mn}, \sigma_{mn}^2} f_1\left(\alpha_{mn}, \mathbf{a}_{mn}, \sigma_{mn}^2\right)}{\prod_{m,n} \max_{\mathbf{a}_{mn}, \sigma_{mn}^2} f_0\left(\mathbf{a}_{mn}, \sigma_{mn}^2\right)}. \quad (5)$$

The maximization of the exact likelihood function with respect to the unknowns is cumbersome. Herein, we use the asymptotic form of the likelihood function [19][1]:

$$f_i = \frac{1}{\left(\pi\sigma_{mn}^2\right)^{(K-P_{mn})}} e^{-\frac{1}{\sigma_{mn}^2} \sum_{k=P_{mn}+1}^{K} |\varepsilon_{mn}(k)|^2}$$

where $i = \{0, 1\}$ specifies H_0 and H_1, respectively, and $\varepsilon_{mn}(k)$ is related to the observation $\mathbf{x}_{mn}$ through (4) and (1). To express the likelihood functions explicitly in terms of the observations $x_{mn}(k)$, let us define[2]

$$\begin{aligned}
\mathbf{x}_{mn} &= [x_{mn}(P_{mn}+1), x_{mn}(P_{mn}+2), \cdots, x_{mn}(K)]^T, \\
\mathbf{s}_{mn} &= [s_{mn}(P_{mn}+1), s_{mn}(P_{mn}+2), \cdots, s_{mn}(K)]^T, \\
\mathbf{y}_{mn}(k) &= [x_{mn}(k-1), x_{mn}(k-2), \cdots, x_{mn}(k-P_{mn})]^T, \\
\mathbf{t}_{mn}(k) &= [s_{mn}(k-1), s_{mn}(k-2), \cdots, s_{mn}(k-P_{mn})]^T, \\
\mathbf{Y}_{mn} &= [\mathbf{y}_{mn}(P_{mn}+1), \mathbf{y}_{mn}(P_{mn}+2), \cdots, \mathbf{y}_{mn}(K)]^T, \\
\mathbf{T}_{mn} &= [\mathbf{t}_{mn}(P_{mn}+1), \mathbf{t}_{mn}(P_{mn}+2), \cdots, \mathbf{t}_{mn}(K)]^T.
\end{aligned}$$

Then, the likelihood function for the (m,n)-th TX-RX pair can be written as

$$\begin{aligned}
f_0 &= \frac{e^{-\frac{1}{\sigma_{mn}^2}\|\mathbf{x}_{mn} + \mathbf{Y}_{mn}\mathbf{a}_{mn}\|^2}}{\left(\pi\sigma_{mn}^2\right)^{K-P_{mn}}}, \\
f_1 &= \frac{e^{-\frac{1}{\sigma_{mn}^2}\|[\mathbf{x}_{mn} + \mathbf{Y}_{mn}\mathbf{a}_{mn}] - \alpha_{mn}[\mathbf{s}_{mn} + \mathbf{T}_{mn}\mathbf{a}_{mn}]\|^2}}{\left(\pi\sigma_{mn}^2\right)^{K-P_{mn}}}. \quad (6)
\end{aligned}$$

It is noted that

$$\tilde{\mathbf{x}}_{mn} \triangleq \mathbf{x}_{mn} + \mathbf{Y}_{mn}\mathbf{a}_{mn}, \quad (7)$$

$$\tilde{\mathbf{s}}_{mn} \triangleq \mathbf{s}_{mn} + \mathbf{T}_{mn}\mathbf{a}_{mn}, \quad (8)$$

represent the *temporally whitened* test signal and, respectively, the *temporally whitened* steering vector by using the AR coefficient $\mathbf{a}_{mn}$.

A. Maximum Likelihood Estimation Under H_1

Here, we derive the MLEs of the unknown parameters under H_1. The ML estimation under H_0 is a special case of that under H_1 by setting $\alpha_{mn} = 0$. The MLEs discussed in the sequel assume knowledge of AR model order P_{mn}. In practice, the ML estimator can be used along with standard model order selection criteria, such as the minimum description length (MDL) criterion or Akaike information criterion (AIC) [19].

From the above likelihood function, the MLE of the variance of the AR driving noise is given by

$$\hat{\sigma}_{mn}^2 = \frac{\|(\mathbf{x}_{mn} + \mathbf{Y}_{mn}\mathbf{a}_{mn}) - \alpha_{mn}(\mathbf{s}_{mn} + \mathbf{T}_{mn}\mathbf{a}_{mn})\|^2}{K - P_{mn}}. \quad (9)$$

Hence, the MLE of α_{mn} is obtained by minimizing

$$\|(\mathbf{x}_{mn} + \mathbf{Y}_{mn}\mathbf{a}_{mn}) - \alpha_{mn}(\mathbf{s}_{mn} + \mathbf{T}_{mn}\mathbf{a}_{mn})\|^2, \quad (10)$$

which yields

$$\hat{\alpha}_{mn} = \frac{(\mathbf{s}_{mn} + \mathbf{T}_{mn}\mathbf{a}_{mn})^H(\mathbf{x}_{mn} + \mathbf{Y}_{mn}\mathbf{a}_{mn})}{(\mathbf{s}_{mn} + \mathbf{T}_{mn}\mathbf{a}_{mn})^H(\mathbf{s}_{mn} + \mathbf{T}_{mn}\mathbf{a}_{mn})}. \quad (11)$$

The likelihood function reduces to (up to a scaling constant)

$$\begin{aligned}
&f_1\left(\hat{\alpha}_{mn}, \mathbf{a}_{mn}, \hat{\sigma}_{mn}^2\right) \\
&\propto \left[(\mathbf{x}_{mn} + \mathbf{Y}_{mn}\mathbf{a}_{mn})^H \mathbf{P}_{mn}^{\perp} (\mathbf{x}_{mn} + \mathbf{Y}_{mn}\mathbf{a}_{mn})\right]^{P_{mn}-K}, \quad (12)
\end{aligned}$$

[1]For notational simplicity, the arguments of the likelihood functions are sometimes suppressed.

[2]For simplicity but some notational abuse, $\mathbf{x}_{mn}$ and $\mathbf{s}_{mn}$ here are formed from the last $K - P_{mn}$ elements of their counterparts in (1).

where

$$\begin{aligned}\mathbf{P}_{mn}^{\perp} &= \mathbf{I} - \frac{(\mathbf{s}_{mn}+\mathbf{T}_{mn}\mathbf{a}_{mn})(\mathbf{s}_{mn}+\mathbf{T}_{mn}\mathbf{a}_{mn})^H}{(\mathbf{s}_{mn}+\mathbf{T}_{mn}\mathbf{a}_{mn})^H(\mathbf{s}_{mn}+\mathbf{T}_{mn}\mathbf{a}_{mn})} \\ &= \mathbf{I} - \frac{\tilde{\mathbf{s}}_{mn}\tilde{\mathbf{s}}_{mn}^H}{\tilde{\mathbf{s}}_{mn}^H\tilde{\mathbf{s}}_{mn}}, \end{aligned} \tag{13}$$

and the second equality is due to (8). From (13), it appears that the projection matrix $\mathbf{P}_{mn}^{\perp}$ is a function of the AR coefficient $\mathbf{a}_{mn}$. In fact, $\mathbf{P}_{mn}^{\perp}$ is independent of $\mathbf{a}_{mn}$ [20]. To see this, we note that the $(k+1)$-st element of $\tilde{\mathbf{s}}_{mn}$, i.e., $\tilde{s}_{mn}(k)$, is a scaled version of $\tilde{s}_{mn}(k)$ [see (8)]

$$\begin{aligned}\tilde{s}_{mn}(k+1) &= s_{mn}(k+1) + \mathbf{t}_{mn}^T(k+1)\mathbf{a}_{mn} \\ &= s_{mn}(k+1) + \sum_{p=1}^{P_{mn}} a_{mn}(p)s_{mn}(k+1-p) \\ &= s_{mn}(k)e^{j2\pi f_{mn}} \\ &\quad + \sum_{p=1}^{P_{mn}} a_{mn}(p)s_{mn}(k-p)e^{j2\pi f_{mn}} \\ &= e^{j2\pi f_{mn}}\tilde{s}_{mn}(k), \end{aligned} \tag{14}$$

where in the third equality, we used the fact that (see (3))

$$s_{mn}(k) = e^{j2\pi(k-1)f_{mn}} = s_{mn}(k+1)e^{-j2\pi f_{mn}}.$$

Therefore, we have

$$\begin{aligned}\tilde{\mathbf{s}}_{mn} &= \tilde{s}_{mn}(P_{mn}+1)\left[1, e^{j2\pi f_{mn}}, \cdots, e^{j2\pi(K-P_{mn}-1)f_{mn}}\right]^T \\ &\triangleq \tilde{s}_{mn}(P_{mn}+1)\boldsymbol{\psi}_{mn}, \end{aligned} \tag{15}$$

where $\boldsymbol{\psi}_{mn}$ is a $(K-P_{mn})\times 1$ Fourier vector. By substituting $\tilde{\mathbf{s}}_{mn}$ into (13), $\mathbf{P}_{mn}^{\perp}$ becomes

$$\begin{aligned}\mathbf{P}_{mn}^{\perp} &= \mathbf{I} - \frac{|\tilde{s}_{mn}(P_{mn}+1)|^2\boldsymbol{\psi}_{mn}\boldsymbol{\psi}_{mn}^H}{|\tilde{s}_{mn}(P_{mn}+1)|^2\boldsymbol{\psi}_{mn}^H\boldsymbol{\psi}_{mn}} \\ &= \mathbf{I} - \frac{\boldsymbol{\psi}_{mn}\boldsymbol{\psi}_{mn}^H}{\boldsymbol{\psi}_{mn}^H\boldsymbol{\psi}_{mn}} \triangleq \mathbf{P}_{\boldsymbol{\psi}_{mn}^{\perp}}. \end{aligned} \tag{16}$$

which is independent of $\mathbf{a}_{mn}$.

Using (16) in (12) and maximizing the resulting likelihood function yield the MLE of $\mathbf{a}_{mn}$

$$\hat{\mathbf{a}}_{mn,1} = -\left(\mathbf{Y}_{mn}^H\mathbf{P}_{\boldsymbol{\psi}_{mn}}^{\perp}\mathbf{Y}_{mn}\right)^{-1}\mathbf{Y}_{mn}^H\mathbf{P}_{\boldsymbol{\psi}_{mn}}^{\perp}\mathbf{x}_{mn}. \tag{17}$$

The likelihood function under H_1 reduces to

$$f_1\big(\mathbf{x}_{mn}|\,\hat{\alpha}_{mn},\hat{\mathbf{a}}_{mn,1},\hat{\sigma}_{mn}^2\big) \propto \left(\mathbf{x}_{mn}^H\mathbf{P}_{\left[\mathbf{P}_{\boldsymbol{\psi}}^{\perp}\mathbf{Y}_{mn}\right]}^{\perp}\mathbf{x}_{mn}\right)^{P_{mn}-K}, \tag{18}$$

where

$$\begin{aligned}\mathbf{P}_{\left[\mathbf{P}_{\boldsymbol{\psi}}^{\perp}\mathbf{Y}_{mn}\right]}^{\perp} &= \mathbf{I} - \mathbf{P}_{\boldsymbol{\psi}_{mn}}^{\perp}\mathbf{Y}_{mn}\left(\mathbf{Y}_{mn}^H\mathbf{P}_{\boldsymbol{\psi}_{mn}}^{\perp}\mathbf{Y}_{mn}\right)^{-1} \\ &\quad \times\mathbf{Y}_{mn}^H\mathbf{P}_{\boldsymbol{\psi}_{mn}}^{\perp}. \end{aligned} \tag{19}$$

The estimates under H_1 are summarized as follows. First, use (17) to compute the MLE $\hat{\mathbf{a}}_{mn,1}$. Second, using $\hat{\mathbf{a}}_{mn,1}$ in (11) gives the MLE $\hat{\alpha}_{mn,1}$. Finally, using $\hat{\mathbf{a}}_{mn,1}$ and $\hat{\alpha}_{mn,1}$ in (9) gives the MLE $\hat{\sigma}_{mn,1}^2$.

B. Maximum Likelihood Estimation Under H_0

By setting $\alpha_{mn}=0$, the MLEs of σ_{mn}^2 and $\mathbf{a}_{mn}$ under H_0 are given by

$$\hat{\mathbf{a}}_{mn,0} = -\left(\mathbf{Y}_{mn}^H\mathbf{Y}_{mn}\right)^{-1}\mathbf{Y}_{mn}^H\mathbf{x}_{mn}, \tag{20}$$

$$\hat{\sigma}_{mn}^2 = \frac{1}{K-P_{mn}}\|\mathbf{x}_{mn}+\mathbf{Y}_{mn}\hat{\mathbf{a}}_{mn,0}\|^2, \tag{21}$$

and the likelihood function under H_0 reduces to

$$f_0\left(\mathbf{x}_{mn}|\,\hat{\mathbf{a}}_{mn,0},\hat{\sigma}_{mn}^2\right) \propto \left(\mathbf{x}_{mn}^H\mathbf{P}_{\mathbf{Y}_{mn}}^{\perp}\mathbf{x}_{mn}\right)^{P_{mn}-K}, \tag{22}$$

where $\mathbf{P}_{\mathbf{Y}_{mn}}^{\perp} = \mathbf{I} - \mathbf{Y}_{mn}(\mathbf{Y}_{mn}^H\mathbf{Y}_{mn})^{-1}\mathbf{Y}_{mn}^H$

C. The MIMO-PGLRT Detector

Using (18) and (22) in (5), we obtain the MIMO-PGLRT detector as follows

$$T_{\mathrm{MIMO-PGLR}} = \prod_{m,n}\left(\frac{\mathbf{x}_{mn}^H\mathbf{P}_{\mathbf{Y}_{mn}}^{\perp}\mathbf{x}_{mn}}{\mathbf{x}_{mn}^H\mathbf{P}_{\left[\mathbf{P}_{\boldsymbol{\psi}}^{\perp}\mathbf{Y}_{mn}\right]}^{\perp}\mathbf{x}_{mn}}\right)^{K-P_{mn}} \underset{H_0}{\overset{H_1}{\gtrless}} \tau \tag{23}$$

where τ is the threshold subject to a preset probability of false alarm. It is seen that the MIMO-PGLRT detector performs local adaptive subspace detection, non-coherent combining using local decision variables, and a global threshold comparison. In particular, the local detector first adaptively projects the test signal into two distinct subspaces: 1) the orthogonal complement of a regression data matrix formed using the returned signal within a CPI (through $\mathbf{P}_{\mathbf{Y}_{mn}}^{\perp}$); and 2) the orthogonal complement of a *target-free* regression data matrix (through $\mathbf{P}_{[\mathbf{P}_{\boldsymbol{\psi}}^{\perp}\mathbf{Y}_{mn}]}^{\perp}$). Then, it computes the energy of both projected test signals, the ratio of which gives the local test variable.

D. Asymptotic Analysis

The exact distributions of the MIMO-PGLRT test variable $T_{\mathrm{MIMO-PGLR}}$ under both hypotheses are rather involved to obtain. We consider instead the asymptotic distribution of $T_{\mathrm{MIMO-PGLR}}$ to offer some insight on its performance. Using the asymptotic result for GLRT (e.g., [24]), we can show that the asymptotic distributions of $T_{\mathrm{MIMO-PGLR}}$ are given by

$$T_{\mathrm{MIMO-PGLR}} \overset{d.}{\sim} \begin{cases}\chi_{2MN}^2, & \text{under } H_0, \\ \chi_{2MN}^2(\xi), & \text{under } H_1. \end{cases} \tag{24}$$

That is, $T_{\mathrm{MIMO-PGLR}}$ is asymptotically a central Chi-square random variable with $2MN$ degrees of freedom under H_0 and, under H_1, a non-central Chi-square random variable with $2MN$ degrees of freedom and non-centrality parameter:

$$\xi = 2\sum_{m,n}\frac{|\alpha_{mn}|^2}{\sigma_{mn}^2}\tilde{\mathbf{s}}_{mn}^H\tilde{\mathbf{s}}_{mn}, \tag{25}$$

where $\tilde{\mathbf{s}}_{m,n} = \mathbf{s}_{m,n} + \mathbf{T}_{m,n}\mathbf{a}_{m,n}$ denotes the whitened steering vector. The derivation of the above non-centrality parameter is shown in Appendix A.

From (24), the probability of false alarm can be written as

$$P_{\rm f} = \mathcal{Q}_{\chi^2_{2MN}}(\tau), \tag{26}$$

where $\mathcal{Q}_{\chi^2_{2MN}}(\cdot)$ is the complementary cumulative distribution function (CDF) of the central Chi-square χ^2_{2MN}. As a result, the threshold τ can be computed as $\tau = \mathcal{Q}^{-1}_{\chi^2_{2MN}}(P_{\rm f})$. The above analysis reveals that asymptotically, the MIMO-PGLR detector under H_0 is statistically independent of the AR-related parameters for disturbance signals, i.e., $\mathbf{a}_{mn}$ and σ^2_{mn}. Therefore, it asymptotically achieves the CFAR property. Meanwhile, the probability of detection can be asymptotically computed as

$$P_{\rm d} = \mathcal{Q}_{\chi^2_{2MN}(\xi)}(\tau), \tag{27}$$

where $\mathcal{Q}_{\chi^2_{2MN}(\boldsymbol{\xi})}(\cdot)$ is the complementary CDF of the non-central Chi-square $\chi^2_{2MN}(\boldsymbol{\xi})$ with $\boldsymbol{\xi}$ given by (25).

E. Unknown Target Velocity

The above discussions are based on the assumption of a given target velocity. In practice, this may correspond to the case when multiple detections are performed on a set of possible values of the target velocity $\mathbf{v}$ or, equivalently, the Doppler frequencies, i.e., $f_{mn} = kf_{\rm PRF}/K, k = 1, 2, \cdots, K$, where $f_{\rm PRF}$ is the pulse repetition frequency. Alternatively, we can treat the target velocity $\mathbf{v}$ as an unknown parameter which needs to be estimated before detection. In this case, the test variable of the MIMO-GLRT detector can be expressed as

$$\max_{\mathbf{v}} \prod_{m,n} \left(\frac{\mathbf{x}^H_{mn}\mathbf{P}^{\perp}_{\mathbf{Y}_{mn}}\mathbf{x}_{mn}}{\mathbf{x}^H_{mn}\mathbf{P}^{\perp}_{\left[\mathbf{P}^{\perp}_{\boldsymbol{\psi}}\mathbf{Y}_{mn}\right]}\mathbf{x}_{mn}} \right)^{K-P_{mn}} \tag{28}$$

where $\mathbf{P}^{\perp}_{[\mathbf{P}^{\perp}_{\boldsymbol{\psi}}\mathbf{Y}_{mn}]}$ is defined in (19). The above maximization depends on $\mathbf{v}$ via $\boldsymbol{\psi}_{mn}$, which is a function of the mn-th Doppler frequency f_{mn} (see (15)) and hence a function of $\mathbf{v}$ (see (2)). The estimation is examined in details in Section IV. The impact of an unknown $\mathbf{v}$ on the detection performance is studied numerically in Section V.

F. Existing Detectors

A recently introduced detector for MTD with distributed MIMO radar is the sample covariance matrix (SCM)-based detector [4], [7]:

$$\max_{\mathbf{v}} \sum_{m,n} \frac{\left|\mathbf{s}^H_{mn}(\mathbf{v})\hat{\mathbf{C}}^{-1}_{mn}\mathbf{x}_{mn}\right|^2}{\mathbf{s}^H_{mn}(\mathbf{v})\hat{\mathbf{C}}^{-1}_{mn}\mathbf{s}_{mn}(\mathbf{v})} \underset{H_0}{\overset{H_1}{\gtrless}} \tau_{\rm SCM} \tag{29}$$

where $\tau_{\rm SCM}$ is the threshold and $\hat{\mathbf{C}}_{mn}$ the sample covariance matrix of the disturbance computed from L *homogeneous* training signals $\mathbf{x}_{mn,\ell} \in \mathbb{C}^{K\times 1}$, $\ell = 1, 2, \cdots, L$, for the (m,n)-th TX-RX pair:

$$\hat{\mathbf{C}}_{mn} = \frac{1}{L}\sum_{\ell=1}^{L} \mathbf{x}_{mn,\ell}\mathbf{x}^H_{mn,\ell}. \tag{30}$$

To ensure that the sample covariance matrix is full rank, $L > K$ range training signals are required for each TX-RX pair. In general, $L = 2K$ training signals are needed for an acceptable performance. As such, the SCM detector (29) requires about $2KMN$ training signals in total, which may be difficult to fulfill in a non-homogeneous environment.

Another detector for MTD with distributed MIMO radar is the robust MIMO detector [10], [25]

$$\max_{\mathbf{v}} \prod_{m,n} \left[1 - \frac{\left|\mathbf{s}^H_{mn}(\mathbf{v})\hat{\mathbf{M}}^{-1}_{mn}\mathbf{x}_{mn}\right|^2}{\left(\mathbf{s}^H_{mn}(\mathbf{v})\hat{\mathbf{M}}^{-1}_{mn}\mathbf{s}_{mn}(\mathbf{v})\right)\left(\mathbf{x}^H_{mn}\hat{\mathbf{M}}^{-1}_{mn}\mathbf{x}_{mn}\right)} \right]^{-K} \underset{H_0}{\overset{H_1}{\gtrless}} \tau_{\rm r-MIMO}, \tag{31}$$

where $\hat{\mathbf{M}}_{mn}$ is a fixed point estimate (FPE) of the covariance matrix obtained by solving [26]–[28]

$$\hat{\mathbf{M}}_{mn} = \frac{K}{L}\sum_{\ell=1}^{L} \frac{\mathbf{x}_{mn,\ell}\mathbf{x}^H_{mn,\ell}}{\mathbf{x}^H_{mn,\ell}\hat{\mathbf{M}}^{-1}_{mn}\mathbf{x}_{mn,\ell}}. \tag{32}$$

The above robust MIMO detector is based on the compound-Gaussian model for the test signals across TX-RX pairs. It requires training signals which follow the same compound-Gaussian model. The FPE (32) can be obtained using an iterative approach [26]–[28].

Compared with the SCM detector and the robust MIMO detector, the proposed MIMO-PGLRT requires no range training signals. The proposed detector is also computationally simpler since the other two detectors require the estimation and inversion of the covariance matrix for each TX-RX pair. Specifically, suppose $P_{\max} \ll K$ where $P_{\max}$ is the maximum AR order and the target velocity is known (the computational cost for target velocity estimation by these methods is similar). The proposed detector has a complexity of $\mathcal{O}(MNP_{\max}K^2)$, while the SCM detector has a complexity of $\mathcal{O}(MN(LK^2 + K^3))$ and the robust MIMO detector has a complexity of $\mathcal{O}(MN(N_{\rm it}LK^2 + K^3))$. The complexity $\mathcal{O}(MNLK^2)$ of the SCM detector and $\mathcal{O}(MNN_{\rm it}LK^2)$ [27] of the robust MIMO detector are due to the covariance matrix estimation in (30) and (32), respectively, where $N_{\rm it}$ denotes the number of iterations in (32), and the complexity $\mathcal{O}(MNK^3)$ is due to the inversion of the $K \times K$ estimated covariance matrix for each TX-RX pair.

IV. Target Velocity Estimation and CRB

In the previous section, the MIMO-PGLRT detector is performed at a set of discrete Doppler frequencies (e.g., uniform samples of the range of unambiguous Doppler frequency) to decide if a moving target is present. The target velocity can be coarsely estimated by inverting (2) from the Doppler frequencies where a target is declared by the detector. In this section, we consider direct and more accurate estimation of the target velocity. For this purpose, we first derive the MLE of the target velocity and then derive the CRB to serve as a benchmark of the estimation performance.

A. ML Estimation of Target Velocity

Following the likelihood function of (18) under H_1, it is readily shown that the MLE of the target velocity is given by

$$\hat{\mathbf{v}} = \arg\min_{\mathbf{v}} \prod_{m,n} \left(\mathbf{x}_{mn}^H \mathbf{P}^{\perp}_{\left[\mathbf{P}^{\perp}_{\boldsymbol{\psi}} \mathbf{Y}_{mn}\right]} \mathbf{x}_{mn} \right)^{K-P_{mn}}, \quad (33)$$

where $\mathbf{P}^{\perp}_{[\mathbf{P}^{\perp}_{\boldsymbol{\psi}}\mathbf{Y}_{mn}]}$ is defined in (19). The cost function in (33) depends on $\mathbf{v}$ via $\boldsymbol{\psi}_{mn}$ in (15), which is a function of the mn-th Doppler frequency f_{mn} (see (15)). The MLE of the target velocity requires a two-dimensional non-linear optimization, which can be solved using numerical approaches. In Section V, we employ a two-step approach to obtain the MLE: a coarse grid search to provide an initial estimate, followed by a refined local search around the initial estimate by using the simplex method. In comparison, the sample-covariance-matrix-based velocity estimator of [4], [7] requires a similar two-dimensional search:

$$\hat{\mathbf{v}}_{\mathrm{SCM}} = \arg\max_{\mathbf{v}} \sum_{m,n} \frac{\left| \mathbf{s}_{mn}^H(\mathbf{v}) \hat{\mathbf{C}}_{mn}^{-1} \mathbf{x}_{mn} \right|^2}{\mathbf{s}_{mn}^H(\mathbf{v}) \hat{\mathbf{C}}_{mn}^{-1} \mathbf{s}_{mn}(\mathbf{v})}, \quad (34)$$

where $\hat{\mathbf{C}}_{mn}$ is defined in (30).

It is known that the mean-squared error (MSE) of the MLE asymptotically achieves the CRB [24]. To provide a benchmark, we derive the corresponding CRB for the target velocity estimation problem.

B. Exact and Asymptotic CRBs

To facilitate the derivation, we employ the transformation rule of the Fisher information matrix (FIM) [8]. Specifically, we first stack all unknown parameters in an $(L+2)\times 1$ vector

$$\boldsymbol{\xi} = \left[v_x, v_y, \boldsymbol{\eta}_{11}^T, \boldsymbol{\eta}_{12}^T, \cdots, \boldsymbol{\eta}_{MN}^T \right]^T, \quad (35)$$

where $L = 3MN + 2\sum_{m,n} P_{mn}$ is the total number of parameters associated with the MN sets of AR processes, and the (m,n)-th parameter set $\boldsymbol{\eta}_{mn} \triangleq [\alpha_{mn}^r, \alpha_{mn}^i, \Re\{\mathbf{a}_{mn}^T\}, \Im\{\mathbf{a}_{mn}^T\}, \sigma_{mn}^2]^T \in \mathbb{R}^{(3+2P_{mn})\times 1}$ including the real and imaginary parts of the complex amplitude α_{mn}, the real and imaginary parts of AR coefficients $\mathbf{a}_{mn}$, and the driving noise variance σ_{mn}^2. Alternatively, the problem can be parameterized by replacing the velocity parameters with the Doppler parameters:

$$\boldsymbol{\theta} = \left[f_{11}, f_{12}, \cdots, f_{MN}, \boldsymbol{\eta}_{11}^T, \boldsymbol{\eta}_{12}^T, \cdots, \boldsymbol{\eta}_{MN}^T \right]^T, \quad (36)$$

where f_{mn} is the Doppler frequency observed at the (m,n)-th TX-RX pair. According to (2), these two sets of parameters are linearly related:

$$\boldsymbol{\theta} = \begin{bmatrix} \mathbf{A} & \mathbf{0} \\ \mathbf{0} & \mathbf{I}_L \end{bmatrix} \boldsymbol{\xi} \triangleq \mathbf{G}\boldsymbol{\xi}, \quad (37)$$

where $\mathbf{I}_L$ is the $L \times L$ identity matrix and the matrix $\mathbf{A} \in \mathbb{R}^{MN\times 2}$ is given by

$$\mathbf{A} = \begin{bmatrix} c_{11} & s_{11} \\ c_{12} & s_{12} \\ \vdots & \vdots \\ c_{MN} & s_{MN} \end{bmatrix} \quad (38)$$

with its elements given by

$$c_{mn} = \frac{T(\cos\theta_{tm} + \cos\theta_{rn})}{\lambda}, \quad (39)$$

$$s_{mn} = \frac{T(\sin\theta_{tm} + \sin\theta_{rn})}{\lambda}. \quad (40)$$

Using the transformation on the FIM [24], we can write the FIM of $\boldsymbol{\xi}$ as follows

$$\mathcal{I}(\boldsymbol{\xi}) = \mathbf{G}^T \mathcal{I}(\boldsymbol{\theta}) \mathbf{G}, \quad (41)$$

where $\mathcal{I}(\boldsymbol{\xi})$ and $\mathcal{I}(\boldsymbol{\theta})$ denote the FIM associated with parameters $\boldsymbol{\xi}$ and $\boldsymbol{\theta}$, respectively. Then, the CRBs of the velocity parameters are the first and second diagonal elements of the inverse of the FIM of $\boldsymbol{\xi}$:

$$\mathrm{var}(\hat{v}_x) \geq \left[\mathcal{I}^{-1}(\boldsymbol{\xi})\right]_{11} = \left[(\mathbf{G}^T \mathcal{I}(\boldsymbol{\theta}) \mathbf{G})^{-1}\right]_{11}, \quad (42)$$

$$\mathrm{var}(\hat{v}_y) \geq \left[\mathcal{I}^{-1}(\boldsymbol{\xi})\right]_{22} = \left[(\mathbf{G}^T \mathcal{I}(\boldsymbol{\theta}) \mathbf{G})^{-1}\right]_{22}. \quad (43)$$

By exploiting the structure of $\mathcal{I}(\boldsymbol{\theta})$ and $\mathbf{G}$, the above CRB expressions can be simplified as (see Appendix B)

$$\mathrm{CRB}(v_x) = \frac{\sum_{mn} s_{mn}^2 \psi_{mn}}{\sum_{mn} c_{mn}^2 \psi_{mn} \sum_{mn} s_{mn}^2 \psi_{mn} - \left(\sum_{mn} c_{mn} s_{mn} \psi_{mn} \right)^2}, \quad (44)$$

$$\mathrm{CRB}(v_y) = \frac{\sum_{mn} c_{mn}^2 \psi_{mn}}{\sum_{mn} c_{mn}^2 \psi_{mn} \sum_{mn} s_{mn}^2 \psi_{mn} - \left(\sum_{mn} c_{mn} s_{mn} \psi_{mn} \right)^2}, \quad (45)$$

where the geometry-related terms c_{mn} and s_{mn} are defined in (39) and (40), respectively, and

$$\psi_{mn} = \mathcal{I}(f_{mn}) - \mathbf{q}_{mn}^T \mathcal{I}^{-1}(\tilde{\mathbf{u}}_{mn}) \mathbf{q}_{mn}. \quad (46)$$

Here, the scalar $\mathcal{I}(f_{mn})$ denotes the Fisher information of the mn-th Doppler frequency f_{mn}, $\mathbf{q}_{mn} = [\mathcal{I}(f_{mn}, \alpha_{mn}^r), \mathcal{I}(f_{mn}, \alpha_{mn}^i)]^T$ denotes the off-diagonal elements of the FIM between the Doppler frequency and the target amplitude, and $\mathcal{I}(\tilde{\mathbf{u}}_{mn}) = \mathcal{I}(\alpha_{mn}^r, \alpha_{mn}^i)$ is a 2×2 sub-matrix of the FIM corresponding to the target amplitude. Additional details of these definitions can be found in Appendix B. From (44) and (45), it is seen that the CRBs of the target velocity estimates mainly depend on two factors. One is the geometry terms c_{mn} and s_{mn} which are explicit functions of the transit-receive antenna configuration, i.e., $\boldsymbol{\theta}_{tm}$ and $\boldsymbol{\theta}_{rn}$. The other is the term $\boldsymbol{\psi}_{mn}$, which is related to the FIM

of the signal parameters, e.g., the Doppler frequency and target amplitude, and hence tied to the SINR.

Given the CRB expressions of (44) and (45), the remaining task is to derive the FIM of $\boldsymbol{\theta}$. In the following, the FIM is given in both the exact and an asymptotic form which, in turn, yield the exact and an asymptotic CRB, respectively, for the velocity parameters.

Exact CRB: In Appendix C, we derive the exact FIM of $\boldsymbol{\theta}$, which can be used to find $\boldsymbol{\psi}_{mn}$ in (44) and (45):

$$\psi_{mn} = 2\frac{|\alpha_{mn}|^2}{\sigma_{mn}^2}\left\|\dot{\mathbf{s}}_{mn} + \dot{\mathbf{T}}_{mn}\mathbf{a}_{mn}\right\|^2\left(1-\frac{1}{\tilde{\mathbf{s}}_{mn}^H\tilde{\mathbf{s}}_{mn}}\right), \quad (47)$$

where $\tilde{\mathbf{s}}_{mn}$ is given by (7), $\dot{\mathbf{s}}_{mn}$ and $\dot{\mathbf{t}}_{mn}(k)$ are, respectively, the first derivatives of $\mathbf{s}_{mn}$ and $\mathbf{t}_{mn}(k)$ with respect to f_{mn} which are given by

$$\dot{\mathbf{s}}_{mn} = -j2\pi\mathbf{P}\odot\mathbf{s}_{mn},$$
$$\dot{\mathbf{t}}_{mn}(k) = -j2\pi\mathbf{P}_k\odot\mathbf{t}_{mn}(k),$$

$\dot{\mathbf{T}}_{mn} = [\dot{\mathbf{t}}_{mn}(P_{mn}+1), \dot{\mathbf{t}}_{mn}(P_{mn}+2), \cdots, \dot{\mathbf{t}}_{mn}(K)]^T$, $\mathbf{P} = [P_{mn}, P_{mn}+1, \cdots, K-1]^T$, $\mathbf{P}_k = [k-2, k-3, \cdots, k-P_{mn}-1]^T$, and $\odot$ denotes the element-wise vector product. Substituting $\boldsymbol{\psi}_{mn}$ of (47) back to (44) and (45) yields the exact CRB for the target velocity. It is seen from (47) that $\boldsymbol{\psi}_{mn}$ is a function of the target amplitude α_{mn}, the steering vector $\mathbf{s}_{mn}$, the AR coefficient $\mathbf{a}_{mn}$, and the driving noise variance σ_{mn}^2. Nevertheless, this expression of $\boldsymbol{\psi}_{mn}$ offers limited intuition; for example, it is unclear how the CRB is related to SINR. In an effort to shed additional light on the problem, we consider next an asymptotic CRB on estimation of $\boldsymbol{\theta}$.

Asymptotic CRB: In Appendix D, we derive an asymptotic form of the FIM on $\boldsymbol{\theta}$, which results in

$$\psi_{mn} = \frac{2\pi^2K^3|\alpha_{mn}|^2}{3\phi_{mn}(-f_{mn})}, \quad (48)$$

where $\phi_{mn}(f)$ denotes the spectrum density of the (m,n)-th AR process:

$$\phi_{mn}(f) = \frac{\sigma_{mn}^2}{\left|1+\sum_{p=1}^{P_{mn}}a_{mn}(p)e^{-j2\pi pf}\right|^2}. \quad (49)$$

It is noted that the AR spectrum density is computed at the frequency of $-f_{mn}$ in (48), i.e., $\phi_{mn}(-f_{mn})$, in accordance with the arrangement of the steering vector in (3). Replacing $\boldsymbol{\psi}_{mn}$ of (48) in (44) and (45) yields an asymptotic CRB for the target velocity. It is seen that the asymptotic expression of $\boldsymbol{\psi}_{mn}$ is directly proportional to the SINR, denoted by $|\alpha_{mn}|^2/\phi_{mn}(f_{mn})$, at the Doppler frequency as seen at the (m,n)-th TX-RX pair, and inversely proportional to K^3, where K is the number of samples at each TX-RX pair. The asymptotic CRB is also notably simpler to compute than the exact counterpart. Numerical results in Section V show that the asymptotic CRB is fairly accurate for moderately small value of K and is a convenient tool.

V. Numerical Evaluation

In this section, numerical results are presented to verify the asymptotic analysis and to demonstrate the performance of the proposed MIMO-PGLRT detector in non-homogeneous clutter environments. The distributed MIMO configuration is shown in Fig. 2, which consists of two transmitters at 0° and 65° relative to the target and two receivers at $-30°$ and 40°. It is noted that the configuration is the same as the one used in [4] and [7]. The pulse repetition frequency is 500 Hz, the carrier frequency is 1 GHz, the target velocity is 108 km/h, and the number of pulses within a CPI is $K = 32$. The above parameters lead to a normalized target Doppler frequency of $|\mathbf{v}|T_{\mathrm{PRI}}/\lambda = 0.2$ in (2).

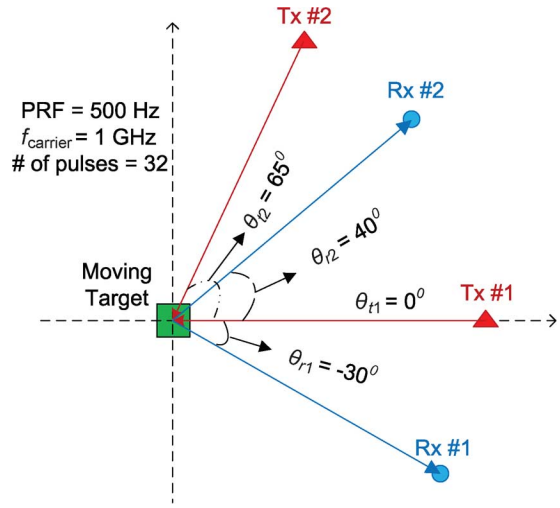

Fig. 2. Distributed MIMO radar configuration used in simulation.

We consider average detection performance averaged over the target moving direction. We examine two different target characteristic cases. In Case A, the moving direction is randomly chosen according to a uniform distribution over the range $[-180°, 180°]$ for each simulation trial, while the target amplitude is kept constant for all TX-RX pairs, i.e., *non-fluctuating* target amplitudes. Case B considers not only a random target moving direction as in Case A but random (*fluctuating*) target amplitude as well. Specifically, the target amplitudes $\alpha_{m,n}$ are generated as complex Gaussian random variables with zero mean and variance $\sigma_{\alpha_{m,n}}^2 = 1$.

A remark on training signals is in order. It is noted that our proposed detector does not use any training signals. However, training signals are required by the detectors discussed in Section III-F. To simulate a non-homogeneous environment, we employ the compound-Gaussian model where the texture component is used to capture the power variation across range resolution cells. Specifically, we use the typical compound-Gaussian model: a K-distributed clutter with a scaling factor of 5 and a shape factor of 0.2. Other than the difference in texture, for each TX-RX pair, the training signals share the same speckle component as the disturbance in the test signal.

A. AR Disturbance

In the first example, we examine the MIMO-PGLRT and the SCM detectors when the disturbances for all TX-RX pairs are generated using independent AR processes. We use the following parameters for the AR models which are randomly picked: (1) $P_{11} = 3$, $\sigma_{11}^2 = 1$, $\mathbf{a}_{11} = [-0.46 - j0.21, -0.17 - j0.2, 0.01 - j0.06]^T$; (2) $P_{12} = 2$, $\sigma_{12}^2 = 0.5$, $\mathbf{a}_{12} = [-0.32 + j0.24, -0.33 + j0.22]^T$;

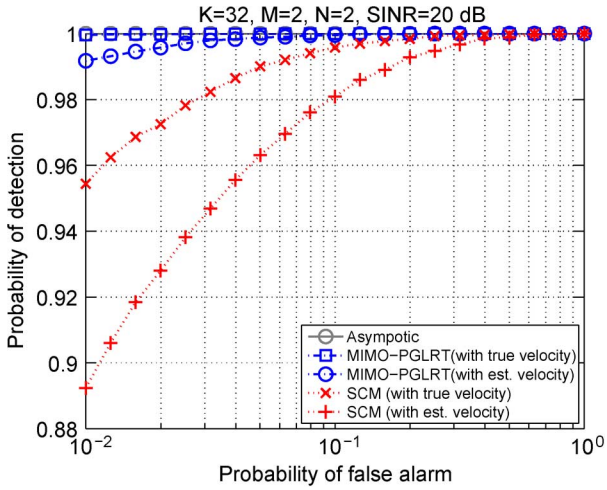

Fig. 3. Receiver-operating-characteristic (ROC) for the MIMO-PGLRT and the SCM detectors with a random target moving direction and non-fluctuating target amplitudes.

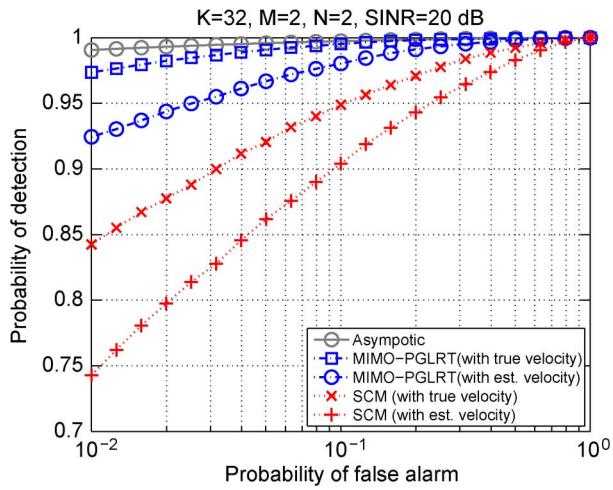

Fig. 4. ROC for the MIMO-PGLRT and the SCM detectors with a random target moving direction and fluctuating target amplitudes.

(3) $P_{21} = 1$, $\sigma_{21}^2 = 2$, $\mathbf{a}_{21} = [-0.1]^T$; (4) $P_{22} = 2$, $\sigma_{22}^2 = 0.8$, $\mathbf{a}_{22} = [-0.34 - j0.31, -0.2 + j0.10]^T$. For the SCM detector, the $L = 2K$ training signals for each TX-RX pair are generated by using the compound-Gaussian model discussed above. The signal-to-interference-plus-noise ratio (SINR) is defined as $\text{SINR} = \sum_{m,n} |\alpha_{mn}|^2 \tilde{\mathbf{s}}_{mn}^H \tilde{\mathbf{s}}_{mn} / \sigma_{mn}^2$ in Case A (non-fluctuating target amplitudes) and $\text{SINR} = \sum_{m,n} \sigma_{\alpha_{mn}}^2 \tilde{\mathbf{s}}_{mn}^H \tilde{\mathbf{s}}_{mn} / \sigma_{mn}^2$ in Case B (fluctuating target amplitudes).

We evaluate the detection performance in both cases of known and unknown target velocity $\mathbf{v} = (v_x, v_y)$. When the target velocity is unknown, the MLE of the target velocity (33) is found by using a two-dimensional nonlinear minimization around an initial estimate, which is chosen to be the true target velocity. A later examination of the impact of the initial velocity estimate on the estimation performance will be considered in Fig. 5. Fig. 3 shows the receiver operating characteristic (ROC) for both the MIMO-PGLRT and the SCM detector in Case A with a random moving direction and non-fluctuating target amplitudes. Also included in the figure is the asymptotic performance derived in Section III-D. The results show that the MIMO-PGLRT, without any range training signals, outperforms the SCM detector which suffers from power variation of the training signals. It is also noted that, with only $K = 32$ temporal (Doppler) samples, the asymptotic result provides a good estimate of the detection performance of the MIMO-PGLRT detector.

Fig. 4 shows the ROC curves for both the MIMO-PGLRT and the SCM detector in Case B with a random moving direction and fluctuating target amplitudes. It is noted that again the MIMO-PGLRT performs better than the SCM detector. By comparing Fig. 4 and Fig. 3, we see a performance loss for both detectors caused by the fluctuating amplitudes.

Next, we evaluate the estimation performance. In this case, the MLE of the target velocity is found in a two-step procedure. First, we perform a two-dimensional grid search to find an initial estimate. Then, a refined minimization of the cost function in (33) is performed around the initial estimate obtained in the first step. Fig. 5 shows the MSE of the MLE (33) and the

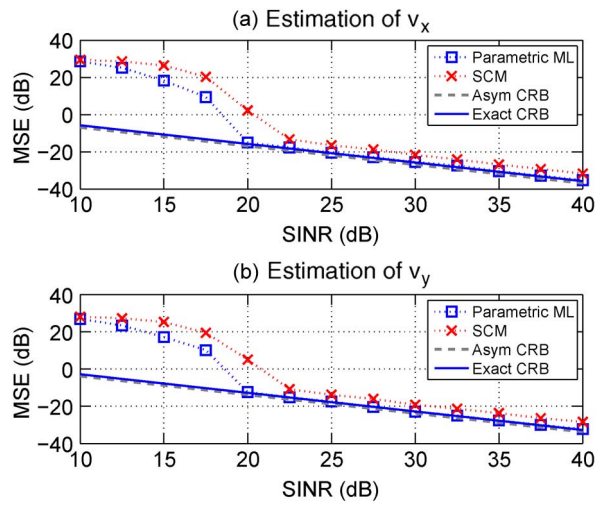

Fig. 5. MSEs of the ML estimator and the SCM estimator, compared with the exact and asymptotic CRBs for the target velocity when $K = 32$.

SCM estimate (34) for v_x and v_y. Both the exact CRBs (47) and asymptotic CRBs (48) are included for comparison. The results show that the MSE of the ML estimator reaches the CRB at high SINR, i.e., above 20 dB in this case. It is also seen that the ML estimator outperforms the SCM estimator (34) which is affected by the non-homogeneous (compound-Gaussian) training signals. Moreover, the asymptotic CRBs provide tight prediction of the exact CRBs: they are both slightly lower than the exact CRBs. As shown in Fig. 6, as the number of samples increases, the asymptotic CRBs approach to the exact CRBs and the deviation between them vanishes.

It should be noted that our CRB is based on the AR Gaussian model as described in Section II, whereby the clutter power of the test signal of each TX-RX antenna pair is a deterministic quantity dictated by the AR coefficients $\{a_{mn}(p)\}$ and noise variance σ_{mn}^2. Our deterministic CRB is suitable for the proposed detector, since it uses only the test signal with fixed clutter power for parameter estimation. In some cases, it might be useful to consider a CRB based on a random clutter power model for the test signal, e.g., K-distributed clutter power, if one is interested in the average performance when estimation

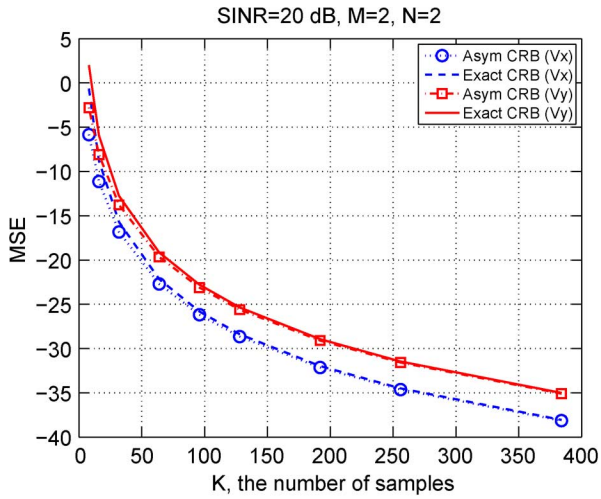

Fig. 6. Comparison of the exact CRBs (47) and asymptotic CRBs (48).

is performed repeatedly across multiple test cells with different (random) clutter power. However, such a stochastic CRB for non-Gaussian clutter cannot be derived in closed form, as shown in [29], [30], where a hybrid/modified CRB was suggested.

B. General Clutter Model

The above results are obtained when the disturbance signals (clutter and noise) are AR processes. In the following, we consider a practical clutter model, which has widely been used to model the clutter Doppler characteristics and is not an AR process [7], [16], to evaluate the performance of the MIMO-PGLRT with model mismatch. Specifically, the clutter temporal correlation function is [7], [16]

$$\Phi(\tau,\varsigma,\delta_v)=\varsigma e^{-8\pi^2\tau^2\frac{\delta_v^2}{\lambda^2}}\triangleq\varsigma\phi(\tau,\delta_v), \tag{50}$$

where ς is the clutter power, τ is the delay, and δ_v is the root mean-square (RMS) of the clutter scatterer velocity. The general clutter covariance matrix $\mathbf{C}$ as a function of ς and δ_v is obtained by sampling the above temporal correlation function at $\tau = kT_{\mathrm{PRI}}, k=0,\cdots,K-1$ [7], [16]:

$$\mathbf{C}(\varsigma,\delta_v)=\varsigma\begin{pmatrix}\rho(0) & \rho(1) & \cdots & \rho(K-1)\\ \rho(1) & \rho(0) & \cdots & \vdots\\ \vdots & \vdots & \ddots & \rho(1)\\ \rho(K-1) & \cdots & \rho(1) & \rho(0)\end{pmatrix}, \tag{51}$$

where $\rho(k)=\phi(kT_{\mathrm{PRI}},\delta_v)$. For the (m,n)-th TX-RX pair, the clutter covariance matrix $\mathbf{R}_{c,mn}$ is generated as $\mathbf{R}_{c,mn}=\mathbf{C}(\varsigma_{mn},\delta_{v,mn})$ according to (51), where ς_{mn} and $\delta_{v,mn}$ denote, respectively, the clutter power and the RMS of scatterer velocity for the (m,n)-th TX-RX pair. In addition to the clutter, a thermal noise component is also present and assumed to be spatially and temporally white Gaussian with zero mean and variance σ_w^2. Overall, the disturbance including the clutter and noise components has a covariance matrix $\mathbf{R}_{d,mn}=\mathbf{R}_{c,mn}+\sigma_w^2\mathbf{I}$. The clutter-to-noise ratio (CNR) is defined as

$$\mathrm{CNR}=\frac{1}{KMN\sigma_w^2}\sum_{m,n}\mathrm{tr}\{\mathbf{R}_{c,mn}\}. \tag{52}$$

The target is simulated according to Case B with a random target moving direction and fluctuating target amplitudes. In this case, the SINR is defined as

$$\mathrm{SINR}=\sum_{m,n}\sigma_{\alpha_{mn}}^2\mathbf{s}_{mn}^H\mathbf{R}_{d,mn}^{-1}\mathbf{s}_{mn}, \tag{53}$$

where $\sigma_{\alpha_{mn}}^2$ is the variance of the fluctuating target amplitude for the (m,n)-th TX-RX pair. In the simulation, the clutter power and the RMS values of the scatterer velocity are, respectively, selected as $\varsigma=[1.5,0.8,2,1]$ and $\delta_v=[0.5,1.5,1.2,0.8]$ m/s for the four TX-RX pairs. The CNR is 30 dB and the SINR is 20 dB.

Similar to the AR dataset, the simulation results are shown in Fig. 7 for both cases of known and unknown target velocity. Also included are the clairvoyant matched filter (MF) which assumes perfect knowledge of the disturbance covariance matrix, the SCM detector (29), and the robust MIMO detector (31). The MF sets a benchmark for the detection performance of all adaptive detectors. For the proposed MIMO-PGLRT detector, we use AR processes with an identical model order $P_{mn}=3$ to model the disturbance seen by different TX-RX pairs. It should be noted that the AR model coefficients $\mathbf{a}_{mn}$ estimated for different TX-RX pairs are still different as the disturbance is non-homogeneous across TX-RX pairs. It is seen from Fig. 7(a), when the training signals are limited, that the MIMO-PGLRT detector without any training signals is still able to suppress the disturbance and provides better detection performance than the SCM detector and the robust MIMO detector using $L=36$ training signals. Specifically, in the limited training case, the robust MIMO detector shows moderate performance loss compared to the proposed MIMO-PGLRT detector, while the SCM detector fails to detect the target. Then we increase the number of training signal from $L=36$ to $L=2K=64$ for each TX-RX pair to simulate a adequate training scenario. As shown in Fig. 7(b), the robust MIMO detector with sufficient training signals shows better detection performance than the proposed MIMO-PGLRT detector whose performance is not affected by the number of training signals. The performance of the SCM detector is also improved but is worse than that of the MIMO-PGLRT detector. It is also noted from the results that the performance gap between the optimal MF and the MIMO-PGLRT detector indicates the effect of model mismatch. Further improvements may be possible by adaptively selecting proper model orders for AR processes, which is a topic of future study.

VI. Conclusion

We have introduced a parametric framework for moving target detection (MTD) in distributed MIMO radar. Within the parametric framework we have developed a MIMO-PGLRT detector and an ML estimator for target velocity estimation. We have explored asymptotic tools to analyze the performance of the MIMO-PGLRT detector, and developed both the exact and an asymptotic CRB, respectively, to lower bound the estimation performance and shed light to the estimation problem. Numerical results show that the proposed detector outperforms the SCM detector in non-homogeneous environments.

The main purpose of this work is to address non-homogeneous clutter which is inherent in distributed MIMO radar due to

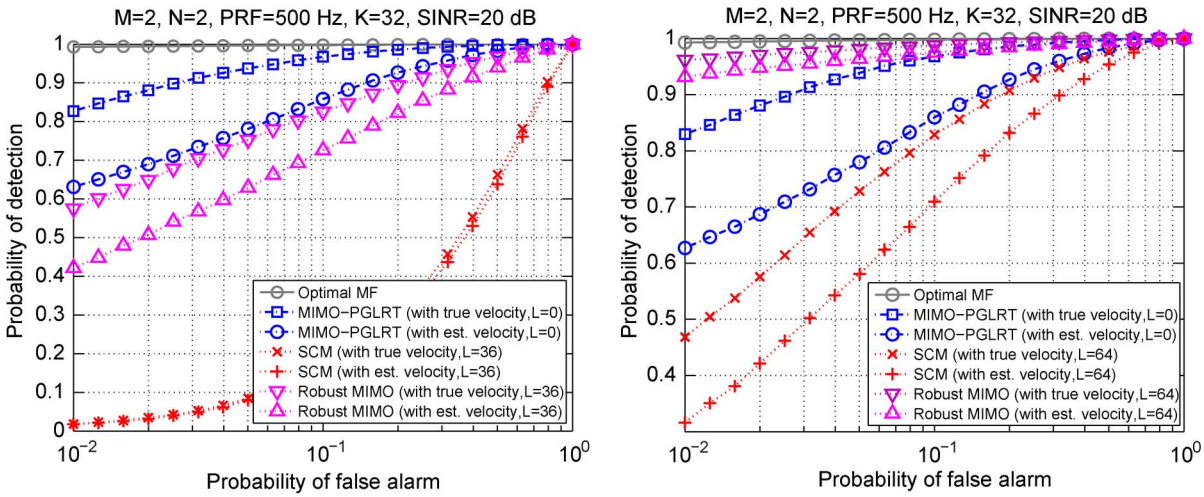

Fig. 7. ROC of the MIMO-PGLRT, the SCM detector and the robust MIMO detector in the general clutter model: (a) $L = 36$ (limited training); (b) $L = 64$ (adequate training).

multi-static TX-RX antenna configurations and azimuth- or direction-selective backscattering of the radar signal in such environments. The proposed parametric approach is not affected by the non-homogeneous clutter variations from cell to cell since it does not rely on range training as the SCM detector. It addresses the non-homogeneity in clutter observed from different TX-RX antennas by using a set of distinctive AR processes for clutter modeling, estimation and cancellation. While numerical results demonstrate that the proposed parametric approach is promising, there are issues to be investigated in the future, such as how to adaptively selecting the AR model order for parametric MTD in distributed MIMO radar.

Appendix A
Proof of (25)

According to [24], the non-centrality parameter is given by

$$\lambda = \left(\boldsymbol{\theta}_{r_1} - \boldsymbol{\theta}_{r_0}\right)^T \left[\mathcal{I}_{\theta_r\theta_r}\left(\boldsymbol{\theta}_{r_0}, \boldsymbol{\theta}_s\right) - \mathcal{I}_{\theta_r\theta_s}\left(\boldsymbol{\theta}_{r_0}, \boldsymbol{\theta}_s\right) \times \mathcal{I}^{-1}_{\theta_s\theta_s}\left(\boldsymbol{\theta}_{r_0}, \boldsymbol{\theta}_s\right) \mathcal{I}_{\theta_s\theta_r}\left(\boldsymbol{\theta}_{r_0}, \boldsymbol{\theta}_s\right)\right] \left(\boldsymbol{\theta}_{r_1} - \boldsymbol{\theta}_{r_0}\right), \quad (54)$$

where $\boldsymbol{\theta}_s = [\sigma_{11}^2, \Re\{\mathbf{a}_{11}\}, \Im\{\mathbf{a}_{11}\}, \cdots, \sigma_{MN}^2, \Re\{\mathbf{a}_{MN}\}, \Im\{\mathbf{a}_{MN}\}]^T$ and $\boldsymbol{\theta}_r = [\Re\{\alpha_{11}\}, \Im\{\alpha_{11}\}, \cdots, \Re\{\alpha_{MN}\}, \Im\{\alpha_{MN}\}]^T$ are the nuisance parameter vector and, respectively, the signal parameter vector, $\mathcal{I}$ denotes the FIM associated with corresponding parameters, $\boldsymbol{\theta}_{r_0} = \mathbf{0}_{2MN\times 1}$ is the signal parameter vector under H_0, and $\boldsymbol{\theta}_{r_1} = \boldsymbol{\theta}_r$ is the signal parameter vector under H_1. Similar to (56) and (57) in Appendix B, we can show that

$$\mathcal{I}_{\theta_s\theta_r} = \mathbf{0}, \quad \mathcal{I}_{\theta_r\theta_s} = \mathbf{0}$$

which simplifies (54) as

$$\lambda = \left(\boldsymbol{\theta}_{r_1} - \boldsymbol{\theta}_{r_0}\right)^T \left[\mathcal{I}_{\theta_r\theta_r}\left(\boldsymbol{\theta}_{r_0}, \boldsymbol{\theta}_s\right)\right] \left(\boldsymbol{\theta}_{r_1} - \boldsymbol{\theta}_{r_0}\right). \quad (55)$$

Using the intermediate results (64), (65) and (66) in Appendix C, we have

$$\mathcal{I}_{\theta_r\theta_r}\left(\boldsymbol{\theta}_{r_0}, \boldsymbol{\theta}_s\right) = \operatorname{diag}\left\{\frac{\tilde{\mathbf{s}}_{11}^H\tilde{\mathbf{s}}_{11}}{\sigma_{11}^2}, \frac{\tilde{\mathbf{s}}_{11}^H\tilde{\mathbf{s}}_{11}}{\sigma_{11}^2}, \cdots, \frac{\tilde{\mathbf{s}}_{MN}^H\tilde{\mathbf{s}}_{MN}}{\sigma_{MN}^2}, \frac{\tilde{\mathbf{s}}_{MN}^H\tilde{\mathbf{s}}_{MN}}{\sigma_{MN}^2}\right\}.$$

Using the above equation along with $\boldsymbol{\theta}_{r_0} = \mathbf{0}_{2MN\times 1}, \boldsymbol{\theta}_{r_1} = \boldsymbol{\theta}_r$, the non-centrality parameter in (55) reduces to (25).

Appendix B
Proof of (44) and (45)

Recall the definition in (36)

$$\boldsymbol{\theta} = \left[f_{11}, f_{12}, \cdots, f_{MN}, \boldsymbol{\eta}_{11}^T, \boldsymbol{\eta}_{12}^T, \cdots, \boldsymbol{\eta}_{MN}^T\right]^T.$$

Rearrange $\boldsymbol{\theta}$ in the order of TX-RX pair

$$\boldsymbol{\theta}' = \left[\boldsymbol{\eta}_{11}'^T, \boldsymbol{\eta}_{12}'^T, \cdots, \boldsymbol{\eta}_{MN}'^T\right]^T,$$

where $\boldsymbol{\eta}_{mn}' = [f_{mn}, \boldsymbol{\eta}_{mn}^T]^T$ includes all unknown parameters corresponding to the (m,n)-th TX-RX pair. Invoking the statistical independence across TX-RX pairs, we have

$$\mathcal{I}(\boldsymbol{\theta}') = \begin{bmatrix} \mathcal{I}\left(\boldsymbol{\eta}_{11}'\right) & \mathbf{0} & \cdots & \mathbf{0} \\ \mathbf{0} & \mathcal{I}\left(\boldsymbol{\eta}_{12}'\right) & \cdots & \mathbf{0} \\ \vdots & \vdots & \ddots & \vdots \\ \mathbf{0} & \mathbf{0} & \cdots & \mathcal{I}\left(\boldsymbol{\eta}_{MN}'\right) \end{bmatrix}.$$

In addition, for a given TX-RX pair, the parameter set $\boldsymbol{\theta}'$ is separated into two subsets: the signal component $\mathbf{u}_{mn} = [f_{mn}, \alpha_{mn}^r, \alpha_{mn}^i]^T$ and the nuisance component $\mathbf{v}_{mn} = [\Re\{\mathbf{a}_{mn}^T\}, \Im\{\mathbf{a}_{mn}^T\}, \sigma_{mn}^2]^T$:

$$\boldsymbol{\eta}_{mn}' = \left[\mathbf{u}_{mn}^T, \mathbf{v}_{mn}^T\right]^T.$$

Using the general formula for the FIM in Gaussian distribution [24], we have

$$\mathcal{I}\left(\boldsymbol{\eta}_{mn}'\right)_{ij} = \operatorname{tr}\left[\mathbf{R}^{-1}{}_{(mn)} \frac{\partial \mathbf{R}(\mathbf{v}_{mn})}{\partial \boldsymbol{\eta}_{mn,i}'} \mathbf{R}^{-1}(\mathbf{v}_{mn}) \frac{\partial \mathbf{R}(\mathbf{v}_{mn})}{\partial \boldsymbol{\eta}_{mn,j}'}\right] + 2\Re\left[\frac{\partial \mathbf{x}_{mn}^H}{\partial \boldsymbol{\eta}_{mn,i}'} \mathbf{R}^{-1}(\mathbf{v}_{mn}) \frac{\partial \mathbf{x}_{mn}}{\partial \boldsymbol{\eta}_{mn,j}'}\right], \quad (56)$$

where $\mathbf{R}(\mathbf{v}_{mn})$ is the covariance matrix for the AR process parameterized by $\mathbf{v}_{mn}$. It is clear from the above equation that the

(m,n)-th diagonal block of the FIM $\mathcal{I}(\boldsymbol{\eta}'_{mn})$ is also block diagonal:

$$\mathcal{I}\left(\boldsymbol{\eta}'_{mn}\right)=\begin{bmatrix}\mathcal{I}(\mathbf{u}_{mn}) & \mathbf{0}\\ \mathbf{0} & \mathcal{I}(\mathbf{v}_{mn})\end{bmatrix}. \tag{57}$$

Since we are only concerned with the estimation of the Doppler frequencies f_{mn}, i.e., the first element of $\boldsymbol{\eta}'_{mn}$ (or, equivalently, $\mathbf{u}_{mn}$), we can move the first element of the diagonal matrices in $\mathcal{I}(\boldsymbol{\theta}')$ to construct an $MN\times MN$ matrix block at the top-left corner of the FIM, which effectively becomes $\mathcal{I}(\boldsymbol{\theta})$

$$\mathcal{I}(\boldsymbol{\theta})=\begin{bmatrix}\mathcal{I}(\mathbf{f}) & \mathbf{D}\\ \mathbf{D}^T & \mathbf{E}\end{bmatrix}, \tag{58}$$

where $\mathcal{I}(\mathbf{f})$ is the FIM of the MN Doppler frequencies, $\mathbf{D}=[\mathbf{D}_{11},\mathbf{D}_{12},\cdots,\mathbf{D}_{MN}]$ with $\mathbf{D}_{mn}$ denoting the off-diagonal elements of the FIM between the MN Doppler frequencies and the (m,n)-th parameters $\boldsymbol{\eta}_{mn}$ including the target amplitude component $\tilde{\mathbf{u}}_{mn}=[\alpha^r_{mn},\alpha^i_{mn}]^T$ and the nuisance component $\mathbf{v}_{mn}$, and

$$\mathbf{E}=\begin{bmatrix}\mathbf{E}_{11} & \cdots & \mathbf{0}\\ \vdots & \ddots & \vdots\\ \mathbf{0} & \cdots & \mathbf{E}_{MN}\end{bmatrix}$$

with

$$\mathbf{E}_{mn}=\begin{bmatrix}\mathcal{I}(\tilde{\mathbf{u}}_{mn}) & \mathbf{0}\\ \mathbf{0} & \mathcal{I}(\mathbf{v}_{mn})\end{bmatrix}. \tag{59}$$

It is noted that the matrix $\mathbf{D}_{mn}$ has a sparse structure:

$$\mathbf{D}_{mn}=\begin{bmatrix}\mathbf{0} & \mathbf{0} & \mathbf{0} & \mathbf{0}\\ \vdots & \vdots & \vdots & \vdots\\ \mathbf{q}^T_{mn} & \mathbf{0} & \mathbf{0} & \mathbf{0}\\ \vdots & \vdots & \vdots & \vdots\\ \mathbf{0} & \mathbf{0} & \mathbf{0} & \mathbf{0}\end{bmatrix}, \tag{60}$$

where $\mathbf{q}_{mn}=[\mathcal{I}(f_{mn},\alpha^r_{mn}),\mathcal{I}(f_{mn},\alpha^i_{mn})]^T$ contains the off-diagonal elements of the FIM between the Doppler frequencies and the real and imaginary parts of the amplitude. This is due to the statistical independence among different TX-RX pairs as well as the diagonal structure of the (m,n)-th FIM sub-matrix. Substituting (58) into (41) yields

$$\mathcal{I}(\boldsymbol{\xi})=\mathbf{G}^T\mathcal{I}(\boldsymbol{\theta})\mathbf{G}=\begin{bmatrix}\mathbf{A}^T\mathcal{I}(\mathbf{f})\mathbf{A} & \mathbf{A}^T\mathbf{D}\\ \mathbf{D}^T\mathbf{A} & \mathbf{E}\end{bmatrix}.$$

Taking the inverse of the above block matrix, we have

$$\mathrm{CRB}(\boldsymbol{\xi})=\begin{bmatrix}\left[\mathbf{A}^T\mathcal{I}(\mathbf{f})\mathbf{A}-\mathbf{A}^T\mathbf{D}\mathbf{E}^{-1}\mathbf{D}^T\mathbf{A}\right]^{-1} & \mathbf{M}_{12}\\ \mathbf{M}_{21} & \mathbf{M}_{22}\end{bmatrix}, \tag{61}$$

where $\mathbf{M}_{12},\mathbf{M}_{21}$ and $\mathbf{M}_{22}$ are matrices for the remaining entries of the CRB which are not of interest here. Therefore, the CRB for the velocity estimation is the first block matrix in (61):

$$\begin{aligned}\mathrm{CRB}(\mathbf{v})&=[\mathrm{CRB}(\boldsymbol{\xi})]_{1:2,1:2}\\ &=\left[\mathbf{A}^T\left(\mathcal{I}(f)-\mathbf{D}\mathbf{E}^{-1}\mathbf{D}^T\right)\mathbf{A}\right]^{-1}.\end{aligned} \tag{62}$$

The term $\mathcal{I}(\mathbf{f})-\mathbf{D}\mathbf{E}^{-1}\mathbf{D}^T$ can be further simplified by using the sparse structure of $\mathbf{D}$ and the block matrix $\mathbf{E}$. Note that

$$\mathbf{D}\mathbf{E}^{-1}\mathbf{D}^T=\sum_{m,n}\mathbf{D}_{mn}\mathbf{E}^{-1}_{mn}\mathbf{D}^T_{mn}.$$

Using (59) and (60), we have

$$\mathbf{D}_{mn}\mathbf{E}^{-1}_{mn}\mathbf{D}^T_{mn}=\mathrm{diag}\left[\mathbf{0},\underbrace{\mathbf{q}^T_{mn}\mathcal{I}^{-1}(\tilde{\mathbf{u}}_{mn})\mathbf{q}_{mn}}_{\text{the }mn\text{-th element}},\mathbf{0}\right].$$

As a result,

$$\begin{aligned}&\mathbf{D}\mathbf{E}^{-1}\mathbf{D}^T\\ &\quad=\mathrm{diag}\left[\mathbf{q}^T_{11}\mathcal{I}^{-1}(\tilde{\mathbf{u}}_{11})\mathbf{q}_{11},\cdots,\mathbf{q}^T_{MN}\mathcal{I}^{-1}(\tilde{\mathbf{u}}_{MN})\mathbf{q}_{MN}\right].\end{aligned}$$

In addition to the diagonal matrix $\mathcal{I}(\mathbf{f})$, we have

$$\mathcal{I}(\mathbf{f})-\mathbf{D}\mathbf{E}^{-1}\mathbf{D}^T=\mathrm{diag}[\psi_{11},\psi_{12},\cdots,\psi_{MN}], \tag{63}$$

where $\boldsymbol{\psi}_{mn}$ is defined in (46). With (63) and the expression of $\mathbf{A}$, we can explicitly express the CRB (62) as (44) and (45).

Appendix C
Proof of (47)

To compute the exact CRB, we need to determine the following entries in the FIM of $\boldsymbol{\theta}$ for $\boldsymbol{\psi}_{mn}$ in (44) and (45):

$$\begin{aligned}\mathcal{I}(f_{mn})&=-E\left[\frac{\partial^2\ln p(\mathbf{x}_{mn})}{\partial f^2_{mn}}\right],\\ \mathbf{q}_{mn}&=\left[\mathcal{I}\left(f_{mn},\alpha^r_{mn}\right),\mathcal{I}\left(f_{mn},\alpha^i_{mn}\right)\right]^T\\ &=\left[-E\left[\frac{\partial^2\ln p(\mathbf{x}_{mn})}{\partial f_{mn}\partial\alpha^r_{mn}}\right],-E\left[\frac{\partial^2\ln p(\mathbf{x}_{mn})}{\partial f_{mn}\partial\alpha^i_{mn}}\right]\right]^T,\\ \mathcal{I}(\tilde{\mathbf{u}}_{mn})&=\begin{bmatrix}\mathcal{I}\left(\alpha^r_{mn}\right) & \mathcal{I}\left(\alpha^r_{mn},\alpha^i_{mn}\right)\\ \mathcal{I}\left(\alpha^r_{mn},\alpha^i_{mn}\right) & \mathcal{I}\left(\alpha^i_{mn}\right)\end{bmatrix}.\end{aligned}$$

With the following intermediate results,

$$\begin{aligned}&\frac{\partial\ln p(\mathbf{x}_{mn})}{\partial\alpha^r_{mn}}\\ &\quad=2\sigma^{-2}_{m,n}\Re\left\{\tilde{\mathbf{s}}^H_{m,n}(\tilde{\mathbf{x}}_{m,n}-\alpha_{m,n}\tilde{\mathbf{s}}_{m,n})\right\}\\ &\frac{\partial\ln p(\mathbf{x}_{mn})}{\partial\alpha^i_{mn}}\\ &\quad=2\sigma^{-2}_{m,n}\Im\left\{\tilde{\mathbf{s}}^H_{m,n}(\tilde{\mathbf{x}}_{m,n}-\alpha_{m,n}\tilde{\mathbf{s}}_{m,n})\right\}\\ &\frac{\partial^2\ln p(\mathbf{x}_{mn})}{\partial\left(\alpha^r_{mn}\right)^2}\\ &\quad=-2\sigma^{-2}_{m,n}\tilde{\mathbf{s}}^H_{m,n}\tilde{\mathbf{s}}_{m,n}\qquad(64)\\ &\frac{\partial^2\ln p(\mathbf{x}_{mn})}{\partial\left(\alpha^i_{mn}\right)^2}\\ &\quad=-2\sigma^{-2}_{m,n}\tilde{\mathbf{s}}^H_{m,n}\tilde{\mathbf{s}}_{m,n}\qquad(65)\\ &\frac{\partial^2\ln p(\mathbf{x}_{mn})}{\partial\alpha^r_{mn}\partial\alpha^i_{mn}}\\ &\quad=2\sigma^{-2}_{m,n}\Re\left\{\tilde{\mathbf{s}}^H_{m,n}(-j\tilde{\mathbf{s}}_{m,n})\right\}=0\qquad(66)\end{aligned}$$

$$\frac{\partial^2 \ln p(\mathbf{x}_{mn})}{\partial \alpha_{mn}^r \partial f_{mn}} = 2\sigma_{m,n}^{-2} \Re\left\{ \frac{\partial \tilde{\mathbf{s}}_{m,n}^H}{\partial f_{mn}} (\tilde{\mathbf{x}}_{m,n} - \alpha_{m,n}\tilde{\mathbf{s}}_{m,n}) - \alpha_{m,n} \frac{\partial \tilde{\mathbf{s}}_{m,n}}{\partial f_{mn}} \right\}$$

$$\frac{\partial^2 \ln p(\mathbf{x}_{mn})}{\partial \alpha_{mn}^i \partial f_{mn}} = 2\sigma_{m,n}^{-2} \Im\left\{ \frac{\partial \tilde{\mathbf{s}}_{m,n}^H}{\partial f_{mn}} (\tilde{\mathbf{x}}_{m,n} - \alpha_{m,n}\tilde{\mathbf{s}}_{m,n}) - \alpha_{m,n} \frac{\partial \tilde{\mathbf{s}}_{m,n}}{\partial f_{mn}} \right\}$$

$$\frac{\partial^2 \ln p(\mathbf{x}_{mn})}{\partial f_{mn}^2} = 2\sigma_{m,n}^{-2} \Re\Bigg\{ -|\alpha_{m,n}|^2 \frac{\partial \tilde{\mathbf{s}}_{m,n}^H}{\partial f_{mn}} \frac{\partial \tilde{\mathbf{s}}_{m,n}}{\partial f_{m,n}} + \alpha_{m,n} \left(\tilde{\mathbf{x}}_{m,n}^H - \alpha_{m,n}^* \tilde{\mathbf{s}}_{m,n}^H \right) \frac{\partial^2 \tilde{\mathbf{s}}_{m,n}}{\partial f_{m,n}^2} \Bigg\},$$

we can show that

$$\mathcal{I}(f_{mn}, \alpha_{mn}^r) = 2\sigma_{m,n}^{-2} \Re\left\{ \alpha_{m,n} (\dot{\mathbf{s}}_{m,n} + \dot{\mathbf{T}}_{m,n} \mathbf{a}_{m,n}) \right\}$$

$$\mathcal{I}(f_{mn}, \alpha_{mn}^i) = 2\sigma_{m,n}^{-2} \Im\left\{ \alpha_{m,n} (\dot{\mathbf{s}}_{m,n} + \dot{\mathbf{T}}_{m,n} \mathbf{a}_{m,n}) \right\}$$

$$\mathcal{I}(f_{mn}) = 2\sigma_{m,n}^{-2} |\alpha_{m,n}|^2 \|\dot{\mathbf{s}}_{m,n} + \dot{\mathbf{T}}_{m,n} \mathbf{a}_{m,n}\|^2,$$

due to $E[\tilde{\mathbf{x}}_{m,n} - \alpha_{m,n}\tilde{\mathbf{s}}_{m,n}] = 0$. With the above result, it is straightforward to show that $\boldsymbol{\psi}_{mn}$ is given by (47).

Appendix D
Proof of (48)

Here we utilize the asymptotic analysis of the estimation of multiple sinusoids in an AR noise [33] to find the asymptotic FIM for our problem. In [33], the estimation problem is parameterized in terms of the angular frequency $\boldsymbol{\omega}_{mn} = -2\pi f_{mn}$, the magnitude $|\alpha_{mn}|$ and the initial phase $\angle\alpha_{mn}$. To utilize the result there, we define $\boldsymbol{\omega} = [\boldsymbol{\omega}_{11}, \boldsymbol{\omega}_{12}, \cdots, \boldsymbol{\omega}_{MN}]^T = -2\pi\mathbf{f}$, and the new amplitude-parameter set $\tilde{\mathbf{u}}_{mn} = [|\alpha_{mn}|, \angle\alpha_{mn}]$ (versus our previous definition of $\tilde{\mathbf{u}}_{mn} = [\alpha_{mn}^r, \alpha_{mn}^i]$), while the nuisance-component set $\mathbf{v}_{mn}$ remains the same. Accordingly, $\mathbf{q}_{mn} = [\mathcal{I}(\boldsymbol{\omega}_{mn}, |\alpha_{mn}|), \mathcal{I}(\boldsymbol{\omega}_{mn}, \angle\alpha_{mn})]^T$ contains off-diagonal entries of the FIM between the Doppler frequencies and the magnitude and, respectively, between the Doppler frequencies and the initial phase. According to [33], the asymptotic FIM for the Doppler frequency, magnitude and initial phase in the AR noise is

$$\mathcal{I}(\mathbf{u}_{mn}) = 2\phi_{mn}^{-1}(\omega_{mn}) \begin{bmatrix} K & 0 & 0 \\ 0 & K|\alpha_{mn}|^2 & \frac{K^2|\alpha_{mn}|^2}{2} \\ 0 & \frac{K^2|\alpha_{mn}|^2}{2} & \frac{K^3|\alpha_{mn}|^2}{3} \end{bmatrix},$$

where $\mathbf{u}_{mn} = [|\alpha_{mn}|, \angle\alpha_{mn}, \boldsymbol{\omega}_{mn}]^T$ and $\phi_{mn}(f)$ denotes the spectral density of the (m,n)-th AR process defined in (49), which results in

$$\mathcal{I}(f_{mn}) = \frac{8\pi^2 K^3 |\alpha_{mn}|^2}{3\phi_{mn}(-f_{mn})}$$

$$\mathcal{I}(\tilde{\mathbf{u}}_{mn}) = 2K\phi_{mn}^{-1}(-f_{mn}) \begin{bmatrix} 1 & 0 \\ 0 & |\alpha_{mn}|^2 \end{bmatrix},$$

$$\mathcal{I}(f_{mn}, |\alpha_{mn}|) = 0,$$

$$\mathcal{I}(f_{mn}, \angle\alpha_{mn}) = \frac{2\pi K^2 |\alpha_{mn}|^2}{\phi_{mn}(-f_{mn})}.$$

As a result, the term $\boldsymbol{\psi}_{mn}$ is

$$\psi_{mn} = \mathcal{I}(f_{mn}) - \mathbf{q}_{mn}^T \mathcal{I}^{-1}(\tilde{\mathbf{u}}_{mn}) \mathbf{q}_{mn} = \frac{2\pi^2 K^3 |\alpha_{mn}|^2}{3\phi_{mn}(-f_{mn})}.$$

References

[1] B. Himed, H. Bascom, J. Clancy, and M. C. Wicks, "Tomography of moving target (TMT)," in *Sensors, Systems, and Next-Generation Satellites*, V. H. Fujisada, J. B. Lurie, and K. Weber, Eds., 2001, vol. 4540, pp. 608–619, Proceedings of SPIE.

[2] D. W. Bliss and K. W. Forsythe, "Multiple-input multiple-output (MIMO) radar and imaging: Degrees of freedom and resolution," in *Proc. 37th Asilomar Conf. Signals, Syst., Comput.*, Pacific Grove, CA, Nov. 2003, vol. 1, pp. 54–59.

[3] E. Fishler, A. M. Haimovich, R. S. Blum, L. J. Cimini, Jr., D. Chizhik, and R. A. Valenzuela, "Spatial diversity in radars—Models and detection performance," *IEEE Trans. Signal Process.*, vol. 54, no. 3, pp. 823–838, Mar. 2006.

[4] A. M. Haimovich, R. S. Blum, and L. J. Cimini, "MIMO radar with widely separated antennas," *IEEE Signal Process. Mag.*, vol. 25, no. 1, pp. 116–129, Jan. 2008.

[5] N. A. Goodman, "Optimum and decentralized detection for multistatic airborne radar," *IEEE Trans. Aerosp. Electron. Syst.*, vol. 43, no. 2, pp. 806–813, Apr. 2007.

[6] H. Godrich, A. Haimovich, and R. Blum, "Target localization accuracy gain in MIMO radar-based systems," *IEEE Trans. Inf. Theory*, vol. 56, no. 6, pp. 2783–2803, Jun. 2010.

[7] Q. He, N. H. Lehmann, R. S. Blum, and A. M. Haimovich, "MIMO radar moving target detection in homogeneous clutter," *IEEE Trans. Aerosp. Electron. Syst.*, vol. 46, no. 3, pp. 1290–1301, Jul. 2010.

[8] Q. He, R. Blum, H. Godrich, and A. Haimovich, "Target velocity estimation and antenna placement for MIMO radar with widely separated antennas," *IEEE J. Sel. Topics Signal Process.*, vol. 4, no. 1, pp. 79–100, Feb. 2010.

[9] Q. He and R. Blum, "Cramer-Rao bound for MIMO radar target localization with phase errors," *IEEE Signal Process. Lett.*, vol. 17, no. 1, pp. 83–86, Jan. 2010.

[10] C. Y. Chong, F. Pascal, J.-P. Ovarlez, and M. Lesturgie, "MIMO radar detection in non-Gaussian and heterogeneous clutter," *IEEE J. Sel. Topics Signal Process.*, vol. 4, no. 1, pp. 115–126, Feb. 2010.

[11] T. Aittomaki and V. Koivunen, "Performance of MIMO radar with angular diversity under Swerling scattering models," *IEEE J. Sel. Topics Signal Process.*, vol. 4, no. 1, pp. 101–114, Feb. 2010.

[12] M. Akcakaya and A. Nehorai, "MIMO radar detection and adaptive design under a phase synchronization mismatch," *IEEE Trans. Signal Process.*, vol. 58, no. 10, pp. 4994–5005, Oct. 2010.

[13] M. Akcakaya and A. Nehorai, "MIMO radar sensitivity analysis for target detection," *IEEE Trans. Signal Process.*, vol. 59, no. 7, pp. 3241–3250, Jul. 2011.

[14] Y. Yang and R. Blum, "Phase synchronization for coherent MIMO radar: Algorithms and their analysis," *IEEE Trans. Signal Process.*, vol. 59, no. 11, pp. 5538–5557, Nov. 2011.

[15] P. Wang, H. Li, and B. Himed, "Moving target detection using distributed MIMO radar in clutter with non-homogeneous power," *IEEE Trans. Signal Process.*, vol. 59, no. 10, pp. 4809–4820, Oct. 2011.

[16] M. I. Skolnik, *Introduction to Radar Systems*, 3rd ed. New York, NY, USA: McGraw-Hill, 2001.

[17] N. J. Willis, *Bistatic Radar,* SciTech Publishing, 2nd ed., 2005.

[18] S. Haykin and A. Steinhardt, *Radar Detection and Estimation*. New York, NY, USA: Wiley, 1992.

[19] S. M. Kay, *Modern Spectral Estimation: Theory and Application*. Englewood Cliffs, NJ, USA: Prentice-Hall, 1988.

[20] A. Sheikhi, M. Nayebi, and M. Aref, "Adaptive detection algorithm for radar signals in autoregressive interference," *Proc. Inst. Electr. Eng.—Radar Sonar Navig.*, vol. 145, no. 5, pp. 309–314, 1998.

[21] J. R. Román, M. Rangaswamy, D. W. Davis, Q. Zhang, B. Himed, and J. H. Michels, "Parametric adaptive matched filter for airborne radar applications," *IEEE Trans. Aerosp. Electron. Syst.*, vol. 36, no. 2, pp. 677–692, Apr. 2000.

[22] G. Alfano, A. De Maio, and A. Farina, "Model-based adaptive detection of range-spread targets," *Proc. Inst. Electr. Eng.—Radar Sonar Navig.*, vol. 151, no. 1, pp. 2–10, Feb. 2004.

[23] M. Greco, F. Bordoni, and F. Gini, "X-band sea-clutter nonstationarity: Influence of long waves," *IEEE J. Ocean. Eng.*, vol. 29, no. 2, pp. 269–283, Apr. 2004.

[24] S. M. Kay, *Fundamentals of Statistical Signal Processing: Detection Theory*. Upper Saddle River, NJ, USA: Prentice-Hall, 1998.
[25] C. Y. Chong, F. Pascal, J. P. Ovarlez, and M. Lesturgie, "Adaptive MIMO radar detection in non-Gaussian and heterogeneous clutter considering fluctuating targets," presented at the IEEE Workshop Statist. Signal Process. (SSP), Cardiff, Wales, U.K., Sep. 2009.
[26] F. Gini and M. Greco, "Covariance matrix estimation for CFAR detection in correlated heavy tailed clutter," *Signal Process.*, vol. 82, no. 12, pp. 1847–1859, Dec. 2002.
[27] E. Conte, A. De Maio, and G. Ricci, "Recursive estimation of the covariance matrix of a compound-Gaussian process and its application to adaptive CFAR detection," *IEEE Trans. Signal Process.*, vol. 50, no. 8, pp. 1908–1915, Aug. 2002.
[28] F. Pascal, Y. Chitour, J. Ovarlez, P. Forster, and P. Larzabal, "Covariance structure maximum- likelihood estimates in compound Gaussian noise: Existence and algorithm analysis," *IEEE Trans. Signal Process.*, vol. 56, no. 1, pp. 34–48, Jan. 2008.
[29] F. Gini, M. Montanari, and L. Verrazzani, "Estimation of chirp radar signals in compound-Gaussian clutter: A cyclostationary approach," *IEEE Trans. Signal Process.*, vol. 48, no. 4, pp. 1029–1039, Apr. 2000.
[30] F. Gini, M. Montanari, and L. Verrazzani, "Maximum likelihood, ESPRIT, and periodogram frequency estimation of radar signals in K-distributed clutter," *Signal Process.*, vol. 80, no. 6, pp. 1115–1126, Jun. 2000.
[31] A. D'Andrea, U. Mengali, and R. Reggiannini, "The modified Cramér-Rao bound and its application to synchronization problems," *IEEE Trans. Commun.*, vol. 42, pp. 1391–1399, Feb./Mar./Apr. 1994.
[32] F. Gini, "A Radar application of a modified Cramér-Rao bound: Parameter estimation in non-Gaussian clutter," *IEEE Trans. Signal Process.*, vol. 46, no. 7, pp. 1945–1953, Jul. 1998.
[33] P. Stoica, A. Jakobsson, and J. Li, "Cisoid parameter estimation in the colored noise case: Asymptotic Cramér-Rao bound, maximum likelihood, and nonlinear least-squares," *IEEE Trans. Signal Process.*, vol. 45, no. 8, pp. 2048–2059, Aug. 1997.

Pu Wang (S'05–M'12) received the B.Eng. and M.Eng. degrees from the University of Electronic Science and Technology of China (UESTC), Chengdu, China, in 2003 and 2006, respectively, and the Ph.D. degree from the Stevens Institute of Technology, Hoboken, NJ, USA, in 2011, all in electrical engineering.

He was an intern at the Mitsubishi Electric Research Laboratories (MERL), Cambridge, MA, USA, in summer 2010. Since May 2011, he has been with the Department of Electrical and Computer Engineering, Stevens Institute of Technology, Hoboken, NJ, USA, where he is a Research Assistant Professor. His current research interests include statistical signal processing, sensor array and multichannel signal processing, (Bayesian) adaptive detection and parameter estimation, time-frequency analysis, and spectrum sensing for cognitive radio networks. He currently holds two U.S. patents.

Dr. Wang received the Outstanding Doctoral Thesis in EE Award in 2011, the Edward Peskin Award in 2011, the Francis T. Boesch Award in 2008, and the Outstanding Research Assistant Award in 2007, all from the Stevens Institute of Technology, and the Excellent Master Thesis in Sichuan Province Award in 2007. He also received the Outstanding Paper Award from IEEE AFRICON 2011.

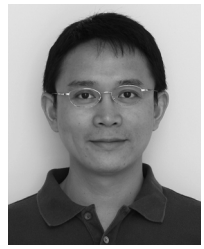

Hongbin Li (M'99–SM'08) received the B.S. and M.S. degrees from the University of Electronic Science and Technology of China, Chengdu, China, in 1991 and 1994, respectively, and the Ph.D. degree from the University of Florida, Gainesville, FL, USA, in 1999, all in electrical engineering.

From July 1996 to May 1999, he was a Research Assistant in the Department of Electrical and Computer Engineering at the University of Florida. He was a Summer Visiting Faculty Member at the Air Force Research Laboratory in summers 2003, 2004, and 2009. Since July 1999, he has been with the Department of Electrical and Computer Engineering, Stevens Institute of Technology, Hoboken, NJ, USA, where he is a Professor. His current research interests include statistical signal processing, wireless communications, and radars.

Dr. Li is a member of Tau Beta Pi and Phi Kappa Phi. He received the Harvey N. Davis Teaching Award in 2003 and the Jess H. Davis Memorial Award for excellence in research in 2001 from Stevens Institute of Technology, and the Sigma Xi Graduate Research Award from the University of Florida in 1999. He is presently a member of the Signal Processing Theory and Methods (SPTM) Technical Committee and served on the Sensor Array and Multichannel (SAM) Technical Committee of the IEEE Signal Processing Society. He was an Associate Editor for the IEEE TRANSACTIONS ON WIRELESS COMMUNICATIONS, IEEE SIGNAL PROCESSING LETTERS, and the IEEE TRANSACTIONS ON SIGNAL PROCESSING, a Guest Editor for the *EURASIP Journal on Applied Signal Processing*, and a General Co-Chair for the Seventh IEEE Sensor Array and Multichannel Signal Processing Workshop, Hoboken, NJ, USA, June 17–20, 2012.

Braham Himed (S'88–M'90–SM'01–F'07) received the B.S. degree in electrical engineering from Ecole Nationale Polytechnique of Algiers in 1984, and the M.S. and Ph.D. degrees, both in electrical engineering, from Syracuse University, Syracuse, NY, in 1987 and 1990, respectively.

He is a Technical Advisor with the Air Force Research Laboratory, Sensors Directorate, RF Technology Branch, Dayton OH, USA, where he is involved with several aspects of radar developments. His research interests include detection, estimation, multichannel adaptive signal processing, time series analyses, array processing, space-time adaptive processing, waveform diversity, MIMO radar, passive radar, and over-the-horizon radar.

Dr. Himed is the recipient of the 2001 IEEE Region I Award for his work on bistatic radar systems, algorithm development, and phenomenology. He is also the recipient of the 2012 Warren White award for excellence in radar engineering. He is a member of the AES Radar Systems Panel.